

Determination of
Martian Surface Reflectivity
From 0.4 to 1.1 Micron
Using a Vidicon Spectrometer

by

Douglas John Mink

Submitted in
Partial Fulfillment
of the Requirements for the
Degree of Master of Science

at the
Massachusetts Institute of Technology

May, 1974

Department of Earth and Planetary Sciences, May 20, 1974

Certified by: _____

Accepted by: _____
Chairman, Departmental Committee on Graduate Students

Determination of Martian Surface Reflectivity from 0.4 to 1.1 Micron
Using a Vidicon Spectrometer

by

Douglas John Mink

Submitted to the Department of Earth and Planetary Science
in partial fulfillment of the requirements for the degree of
Master of Science on May 23, 1974

ABSTRACT

A new astronomical instrument, the vidicon spectrometer, is being developed at the M.I.T. Planetary Astronomy Laboratory. Based on the silicon diode vidicon system currently in use there, a low dispersion prism is added between the vidicon image tube and the telescope, allowing digital vidicon photographs to be taken of spectra. These spectra are stored on magnetic tape and computer processed to create intensity vs. wavelength curves for stars and planets. The high spatial resolution of the vidicon image tube, combined with a higher spectral resolution than photometer filters currently in use at M.I.T. give this instrument potential in the study of planetary surface composition from spectral reflectivity. Procedures for reducing the vidicon images to spectra have been tested on a set of spectra of two stars and the planet Mars. It is concluded that the vidicon response is not linear enough with variations in exposure time at low levels of incoming light for consistent star spectra, although it works well with Mars due to the planet's larger intensity where the vidicon tube has its poorest response. The spectrometer slit is so narrow (one second of arc for this data) that wavelength-dependent variations in refraction of light from a point source by the atmosphere cause star spectra of variable quality. Because of the low quality of the star spectra, direct spectral reflectivity measurements (which are obtained using Mars to star ratios) proved to be impossible. Although further tests of the spectral and intensity response of the silicon diode vidicon should be carried out in the laboratory before good results can be guaranteed, the present Mars spectra may probably be used in conjunction with photometer-derived reflectivity data to expand coverage of the surface of Mars.

Thesis Advisor: Thomas B. McCord

Title: Associate Professor of Planetary Physics

Acknowledgements

Numerous people were involved in the design and construction of the vidicon spectrometer, although I have only met a few. Professor Thomas B. McCord, Mr. Jeffrey Bosel, and Ms. Carle Pieters have been informative about the design of the hardware, as well as the conditions under which they obtained the Mauna Kea data. Dr. Robert Huguenin lent his insight into the problems of Martian surface composition, as well as criticizing an early draft of this thesis. Steve Kent, who is also working with the spectrometer, provided criticism and astronomical knowledge. My spouse, Catherine, has greatly aided me financially and morally, while David McDonald greatly expedited the production of this thesis, with the aid of several computers.

Table of Contents

- I. Introduction _____ page 5
- II. The Vidicon Spectrometer _____ page 9
- III. Image Processing _____ page 16
- IV. Analysis of Data _____ page 27
- V. Recommendations for Future Use _____ page 50

I. Introduction

Although Mariner 9 has returned a vast quantity of information about the planet Mars, little was learned about surface composition. From such experiments as the infrared spectrometer, particle size and silica composition were estimated, but these determinations had error bars so great as to be nearly useless in reaching conclusions about the composition of the surface materials of Mars. Until the Viking Lander in 1976, there is no way to physically look at a Martian rock with instruments.

Probably the most useful technique for remotely sensing surface composition is reflectance spectroscopy. Dollfus (1961), studying the polarization of light reflected by Mars, concluded that limonite, a hydrated iron oxide, was probably a major constituent. Hovis (1965) observed absorption bands in the near-infrared reflectivity of limonite and suggested that they would be a diagnostic test for limonite on Mars. Sagan et al (1965) compared absorption bands they observed in laboratory specimens of limonite to Dollfus' Martian albedo curves and concluded that a surface with at least some limonite was not inconsistent with the data. Adams (1968) observed absorption bands between 0.5 and 2.5 microns in many iron-bearing minerals, the positions of which varied significantly from mineral to mineral. These bands are caused by electron transitions in iron ions and by vibrational bands in hydroxyl ions and water molecules. Adams suggests that

the absorption feature observed in Tull's (1966) geometric albedo curve is not inconsistent with a hydrated basalt composition. The feature observed at one micron in their spectra is not due to iron in iron oxides, but to iron ions in silicates. Adams and McCord (1969), using geometric albedoes obtained during the 1967 opposition discovered that curves for the bright areas had different shapes than those from the dark areas of the Martian surface. They concluded that the surface was composed of a combination of oxidized basalt and hydrated iron oxides. The bright and dark areas were modelled as being composed of the same material in different degrees of oxidation.

McCord and Westphal (1971, see also McCord, Elias, and Westphal, 1971) observed Mars during the 1969 opposition and noted that the iron ion absorptions were in different places, indicating compositional differences. Seven areas were observed, four dark and three bright, each being about five Martian longitudinal degrees in diameter. From this data, much compositional analysis has been done (see Figure 1 for examples of mineral reflectivities compared to Mars); however, from such a small sample, generalizations about the rest of the surface cannot be made. Despite over twenty additional spots obtained during the 1973 opposition, such interesting features as the Coprates canyon and the Hellas basin remain uncovered; what is needed is whole disk coverage at high spectral and spatial resolution. A new technique, vidicon spectroscopy, has been developed to obtain the

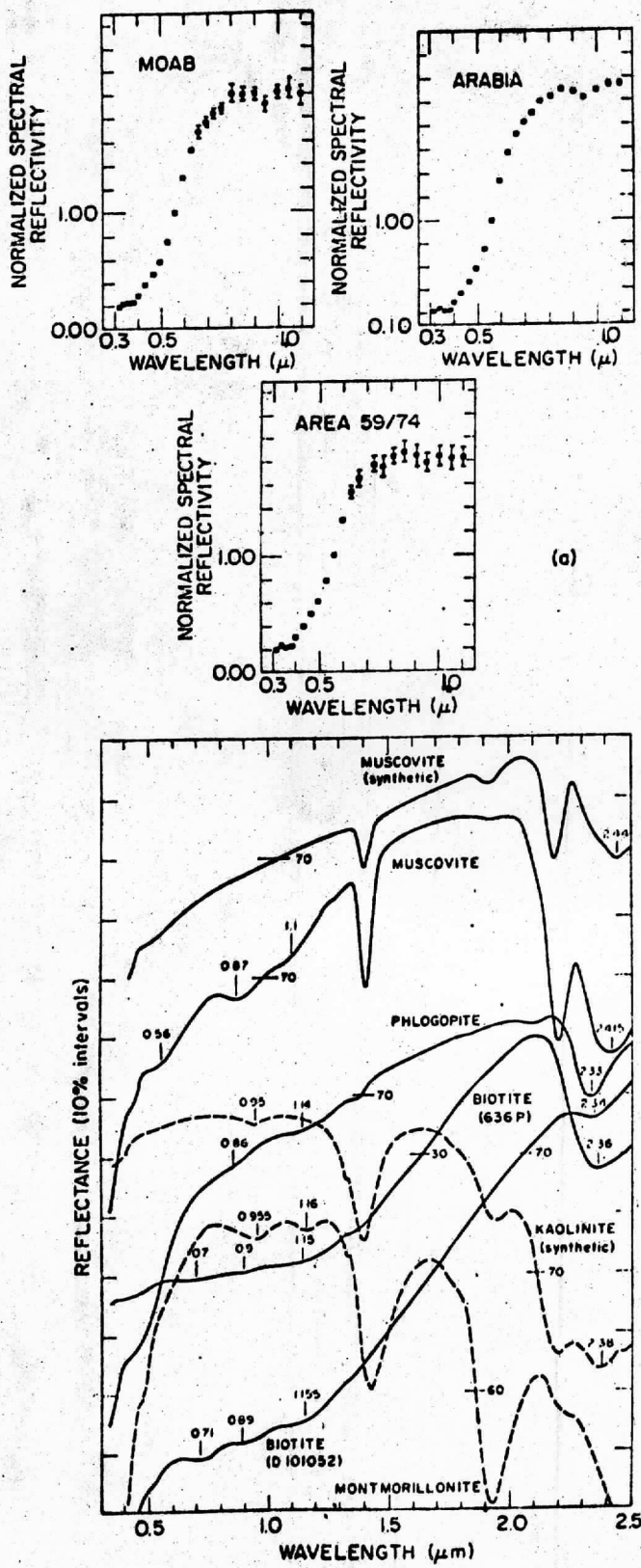


Figure 1.

Comparison of Mars dark area reflectivity to reflectivity of sheet silicates. Note resemblance to the clay minerals, kaolinite and montmorillonite.

(Courtesy Dr. Robert Huguenin)

desired high resolution full-disk coverage. This thesis describes that technique.

II. The Vidicon Spectrometer

The silicon diode array vidicon was originally developed for television and picturephone use, but because of its large dynamic range, high quantum efficiency, and linear response, it is being used by a growing number of astronomers as a digital replacement for photographic plates. The only advantage a photographic plate has over a vidicon is spatial resolution; however, that is not a limiting factor as atmospheric conditions are the resolution-limiting factor in astronomy. McCord and Westphal (1972), Kunin (1972), and McCord and Bosel (1973) have reported on the development of a vidicon system for single-frame astronomical photography at the Planetary Astronomy Laboratory of the Massachusetts Institute of Technology (MITPAL). This system is based on an RCA silicon vidicon tube with a peak quantum efficiency of 85% at 0.5 microns, sloping off to about 6% at 1.1 microns (see Figure 2). Using filters this system has been developed as a two-dimensional imaging photometer, using filter sets similar to those used with photometers for spectral reflectivity work at MIT. As reported by McCord and Bosel, a vidicon spectrometer which would give the spatial resolution of the vidicon combined with a greater spectral resolution than such a vidicon photometer is under development.

The vidicon spectrometer is basically an optical system which is attached to the front end of the vidicon system on the telescope. Schematically it consists of a low-dispersion prism

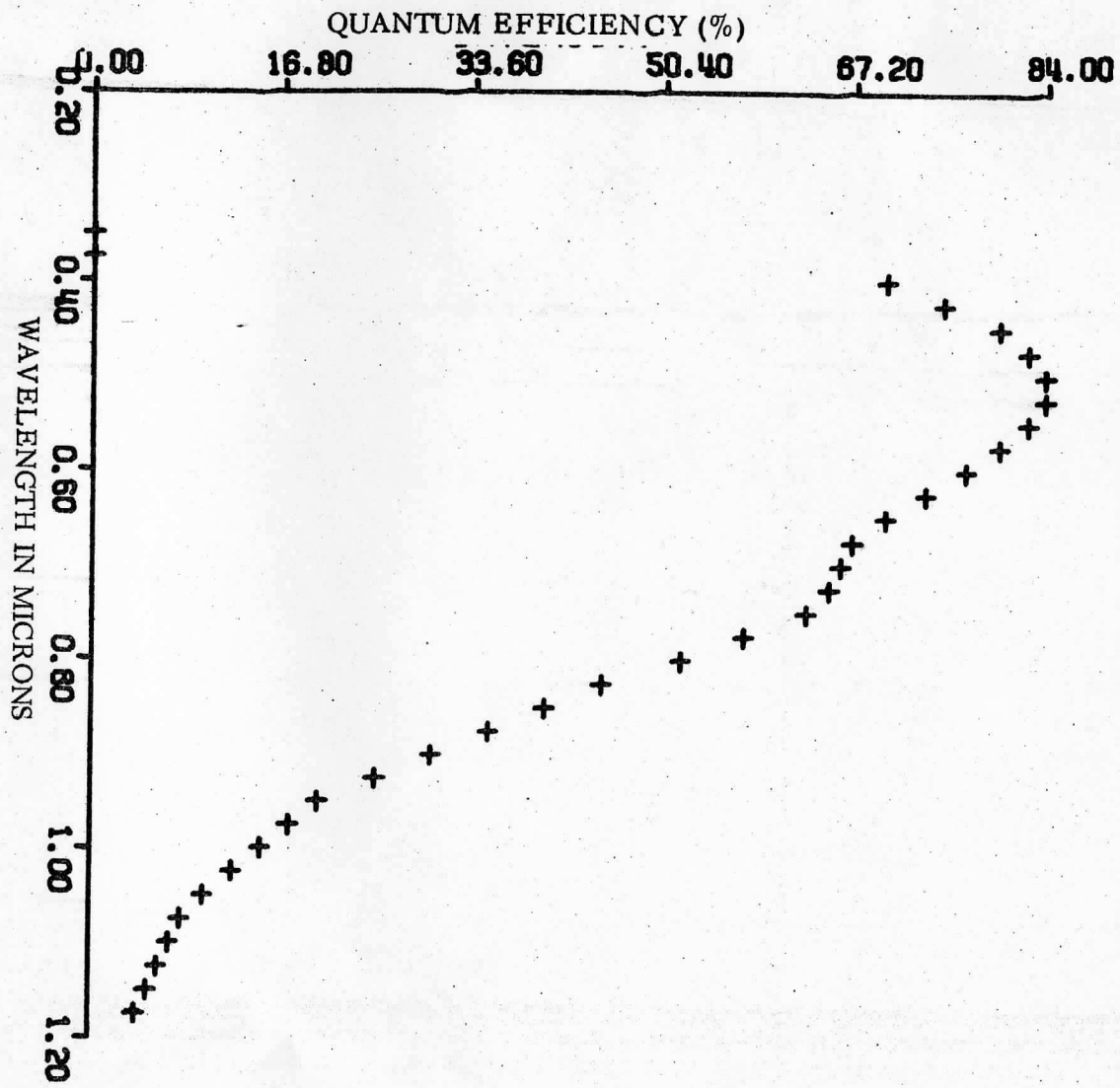


Figure 2. Quantum efficiency of the RCA vidicon. This is the percentage of incoming photons which the diode array and affect it as opposed to being reflected or passing through without being absorbed. This graph was made by averaging the published curve over 250 angstrom segments.

through which light from a slit situated at the focus of the telescope is passed. The dispersed image of the slit is then refocused onto the surface of the vidicon diode array. In practice this is done through a system of mirrors (see Figure 3 for details) to avoid the infrared absorption of lenses.

The vidicon tube consists of a 1024 by 1024 array of reverse biased diodes. A photon impinging on the vidicon target results in a decrease in charge in the diode it reaches. The image is read out by scanning the diode array with an electron beam which recharges the diodes as it hits them, producing a current proportional to the amount of charge lost. By knowing where the beam is at any given time, the intensity at each location in the diode array can be known. These intensity elements are then passed on to be recorded and displayed (for further details on the electronics of a silicon vidicon see Crowell and Labuda (1963)). The vidicon is read out as 250 rows of 256 image elements, each of which corresponds physically to four diodes. In such a lower resolution scan, less accurate positioning is required of the electron beam. No data is lost, and the vidicon's resolution is still better than the atmosphere allows. The intensity image is amplified, recorded on magnetic tape, and displayed on a slow scan TV monitor. This image is then available for further computer processing. The spectrometer system is diagrammed in Figure 4.

A portion of a vidicon spectrometer image is presented in Figure 5. The elements along the column correspond to spatial

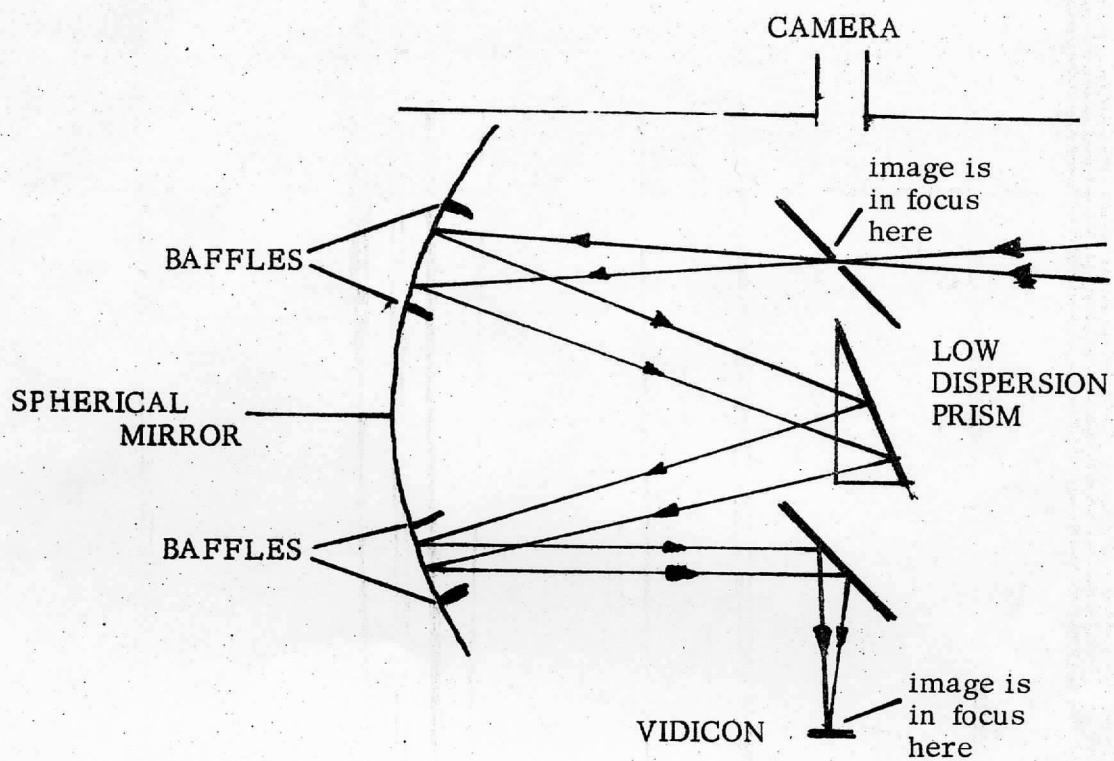


Figure 3. Optics of the MITPAL vidicon spectrometer.
The telescope is to the right.

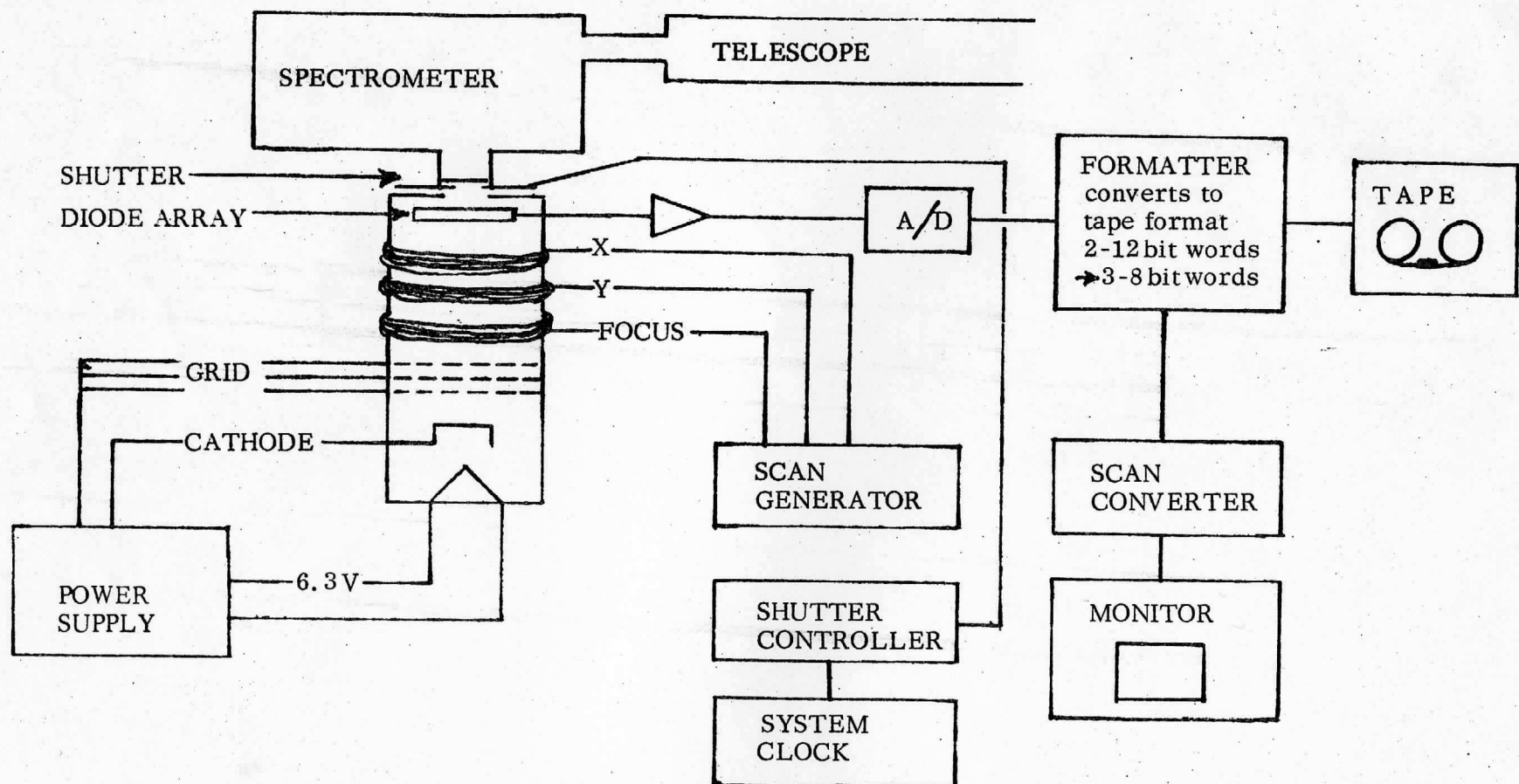


Figure 4. The MITPAL vidicon system with the spectrometer attached.

elements along the slit. Wavelength is along the abscissa. The magnitude of each element is proportional to the current from the vidicon diode array at the time a corresponding diode was read by the scanning electron beam. The image is now ready to be turned into a spectrum.

PART I		176	177	178	179	180	181	182	183	184	185	186	187	188	189	190	191	192	193	194	195	196	197	198	199	200
1-	557	553	564	567	559	553	564	567	560	559	547	550	559	558	556	556	554	565	556	552	558	557	546	549	555	
2-	245	255	240	245	243	253	247	244	241	242	240	243	240	240	238	239	246	239	240	245	252	238	246	243	240	
3-	169	184	193	190	187	192	193	190	186	190	189	188	179	183	191	188	186	195	186	196	192	187	198	189	191	
4-	165	161	161	173	171	162	164	171	181	174	162	175	166	156	167	165	163	161	176	164	172	172	156	165	164	
5-	139	161	127	152	155	157	167	164	164	152	158	170	166	159	153	157	150	157	164	158	170	169	169	172	175	
6-	158	159	156	152	157	155	166	157	160	155	160	163	159	163	161	165	163	166	157	162	157	175	176	156	185	
7-	146	139	157	147	154	155	152	158	151	144	149	158	151	157	147	144	159	157	167	159	165	163	171	169	173	
8-	157	149	156	150	159	153	157	163	158	155	162	145	157	153	157	153	155	170	167	166	175	176	179	165	176	
9-	151	162	159	154	161	163	151	152	154	160	163	159	153	170	159	181	165	170	172	179	181	180	194	181	179	
10-	165	162	170	165	172	183	176	162	170	157	176	173	171	160	172	179	174	180	187	183	181	189	184	194	194	
11-	218	192	208	215	209	199	202	209	199	210	209	212	202	210	202	219	206	209	209	203	205	197	199	208	200	
12-	341	354	343	361	358	347	350	354	337	325	322	327	311	295	298	300	284	273	258	245	242	240	237	226	228	
13-	590	606	613	616	625	630	627	629	607	573	570	557	552	535	506	476	452	422	380	347	325	317	301	299	267	
14-	638	662	653	653	653	669	677	645	659	660	654	653	645	614	591	572	523	473	431	409	391	375	347	312		
15-	1243	1273	1283	1267	1265	1269	1276	1245	1190	1144	1127	1131	1099	1047	1012	972	919	848	735	646	609	582	545	472	417	
16-	2089	2119	2149	2126	2147	2179	2191	2172	2099	2048	2047	2040	2016	1950	1878	1795	1711	1562	1311	1165	1102	1035	935	805	653	
17-	2411	2453	2405	2500	2520	2555	2567	2549	2484	2439	2425	2439	2417	2360	2304	2219	2123	1967	1687	1541	1506	1498	1295	1120	959	
18-	2461	2515	2512	2311	2550	2604	2625	2617	2540	2487	2491	2484	2459	2416	2323	2285	2185	2042	1788	1648	1625	1568	1449	1291	1111	
19-	2425	2471	2473	2504	2503	2544	2567	2547	2489	2433	2444	2449	2417	2357	2297	2228	2138	2019	1768	1647	1607	1551	1457	1309	1136	
20-	2399	2439	2455	2460	2477	2912	2540	2534	2460	2401	2408	2397	2377	2304	2271	2207	2112	1968	1750	1615	1583	1547	1427	1279	1138	
21-	2113	2359	2314	2384	2397	2430	2459	2450	2384	2339	2360	2356	2324	2265	2201	2127	1932	1706	1567	1558	1497	1388	1242	1094		
22-	2163	2203	2224	2232	2241	2230	2312	2103	2275	2189	2194	2200	2185	2129	2075	2001	1927	1811	1616	1489	1455	1420	1311	1191	1043	
23-	2176	2272	2225	2165	2225	2326	2311	2328	2273	2225	2204	2222	2208	2190	2080	2023	1939	1823	1611	1477	1444	1411	1311	1165	1031	
24-	2311	2325	2337	2347	2448	2671	2488	2496	2432	2368	2352	2368	2304	2236	2179	2097	1963	1721	1590	1549	1503	1381	1236	1070		
25-	2142	2215	2225	2227	2643	2704	2747	2733	2656	2592	2587	2611	2592	2507	2456	2403	2321	2175	1902	1748	1712	1673	1532	1363	1195	
26-	2443	2474	2474	2511	2508	2504	2541	2666	2621	2613	2556	2665	2553	2496	2424	2357	2272	2111	1904	1752	1723	1678	1581	1467	1235	
27-	2715	2745	2777	2701	2816	2940	2880	2880	2816	2748	2744	2732	2723	2675	2601	2529	2452	2313	2044	1900	1869	1805	1691	1527	1351	
28-	2954	3006	3129	3129	3051	3116	3151	3159	3073	3017	3021	3045	3041	2960	2869	2816	270d	2570	2268	2043	2073	2028	1888	1683	1480	
29-	2947	3202	3121	3055	3073	3127	3160	3191	3113	3040	3056	3075	3057	2992	2920	2841	2776	2609	2303	2121	2109	2062	1919	1744	1535	
30-	3102	3141	3127	3141	3152	3208	3268	3268	3208	3184	3112	3121	3139	3120	3056	2992	2929	2800	2686	2345	2156	2147	2108	1965	1793	1568
31-	2889	2746	3009	3052	3120	3168	3192	3124	3045	3052	3064	3058	2971	2912	2835	2752	2631	2309	2143	2101	2047	1900	1724	1531		
32-	2805	2812	2401	2136	2937	3006	3043	3066	3041	2955	2941	2969	2944	2881	2805	2709	2631	2520	2232	2053	2017	1951	1829	1665	1470	
33-	2679	2768	2870	2817	2940	2911	2916	2976	2935	2861	2858	2865	2848	2776	2689	2617	2549	2471	2145	1971	1936	1907	1763	1605	1427	
34-	2307	2354	2421	2461	2488	2502	2589	2589	2565	2499	2510	2544	2524	2467	2418	2334	2245	2119	1866	1732	1712	1681	1565	1429	1268	
35-	1922	2230	2037	2072	2381	202L	2126	2113	2083	2035	2043	2057	2034	1996	1936	1887	1333	1740	1555	1444	1415	1386	1289	1191	1067	
36-	2323	2367	2421	2451	2469	2471	2535	2548	2496	2432	2435	2444	2432	2384	2319	2249	2164	2055	1786	1631	1599	1567	1463	1363	1143	
37-	2547	2503	2549	2552	2579	2612	2661	2659	2621	2572	2559	2573	2563	2504	2439	2382	2315	2201	1950	1763	1710	1686	1571	1421	1243	
38-	2525	2580	2617	2638	2657	2716	2766	2765	2647	2651	2665	2627	2571	2536	2480	2404	2298	2018	1843	1827	1777	1652	1476	1293		
39-	2345	2423	2491	2471	2502	2564	2603	2613	2721	2512	2501	2544	2528	2366	2303	2179	1932	1784	1774	1741	1617	1466	1279			
40-	2493	2543	2593	2611	2647	2635	2741	2768	2721	2643	2641	2652	2534	2456	2411	2305	2032	1880	1855	1803	1677	1517	1324			
41-	2337	2423	2427	2461	2494	2544	2577	2527	2540	2464	2481	2535	2528	2465	2503	2327	2276	2195	1924	1757	1765	1724	1613	1456	1279	
42-	2416	2592	2533	2536	2617	2647	2676	2621	2569	2565	2607	2606	2544	2471	2412	2346	2240	1976	1819	1793	1768	1654	1483	1308		
43-	2339	2401	2435	2447	2442	2551	2549	2604	2562	2505	2524	2560	2547	2502	2432	2373	2292	2208	1925	1787	1761	1736	1609	1451	1295	
44-	2194	2256	2300	2313	2332	2391	2433	2456	2395	2347	2357	2393	2381	2329	2289	2233	2160	2055	1819	1673	1651	1614	1505	1368	1228	
45-	2149	2111	2163	2195	2195	2247	2262	2262	2217	2224	2240	2235	2172	2113	2071	2012	1921	1681	1544	1526	1494	1389	1294	1115		
46-	2171	2141	1961	1899	1919	1948	1955	1955	1920	1887	1897	1907	1919	1909	1876	1811	1769	1718	1642	1454	1335	1328	1276	1197	1087	963
47-</																										

III. Image Processing

The first processing that must be done to the image is to convert the column coordinate into wavelength. This is done through the use of a calibration function:

$$S = -S_0 + \frac{C}{(\lambda - \lambda_0)} \quad \lambda = \lambda_0 + \frac{C}{(S + S_0)}$$

S_0 , λ_0 , and C being three constants determined from three column number-wavelength correspondences as follows:

$$C = \frac{(\lambda_1 - \lambda_2)(S_1 + S_0)(S_2 + S_0)}{(S_2 - S_1)}$$

$$S_0 = -S_1 + \frac{(\lambda_2 - \lambda_3)(S_2 - S_1)(S_3 - S_1)}{(\lambda_1 - \lambda_2)(S_3 - S_2) - (\lambda_2 - \lambda_3)(S_2 - S_1)}$$

$$\lambda_0 = \lambda_1 - \frac{C}{(S_1 + S_0)}$$

These correspondences are obtained by observing the spectrometer image of a calibration lamp with known sharp emission lines (as shown in Figure 6). From this calibration, which is redone periodically as data is taken, the wavelength-column relationship is known (see Figure 7 for an example). The resolution also varies as a function of wavelength, as would be expected (see Figure 8 for a sample dispersion function plotted from the first derivative of the calibration function).

Now enough is known to process a spectral image. A program

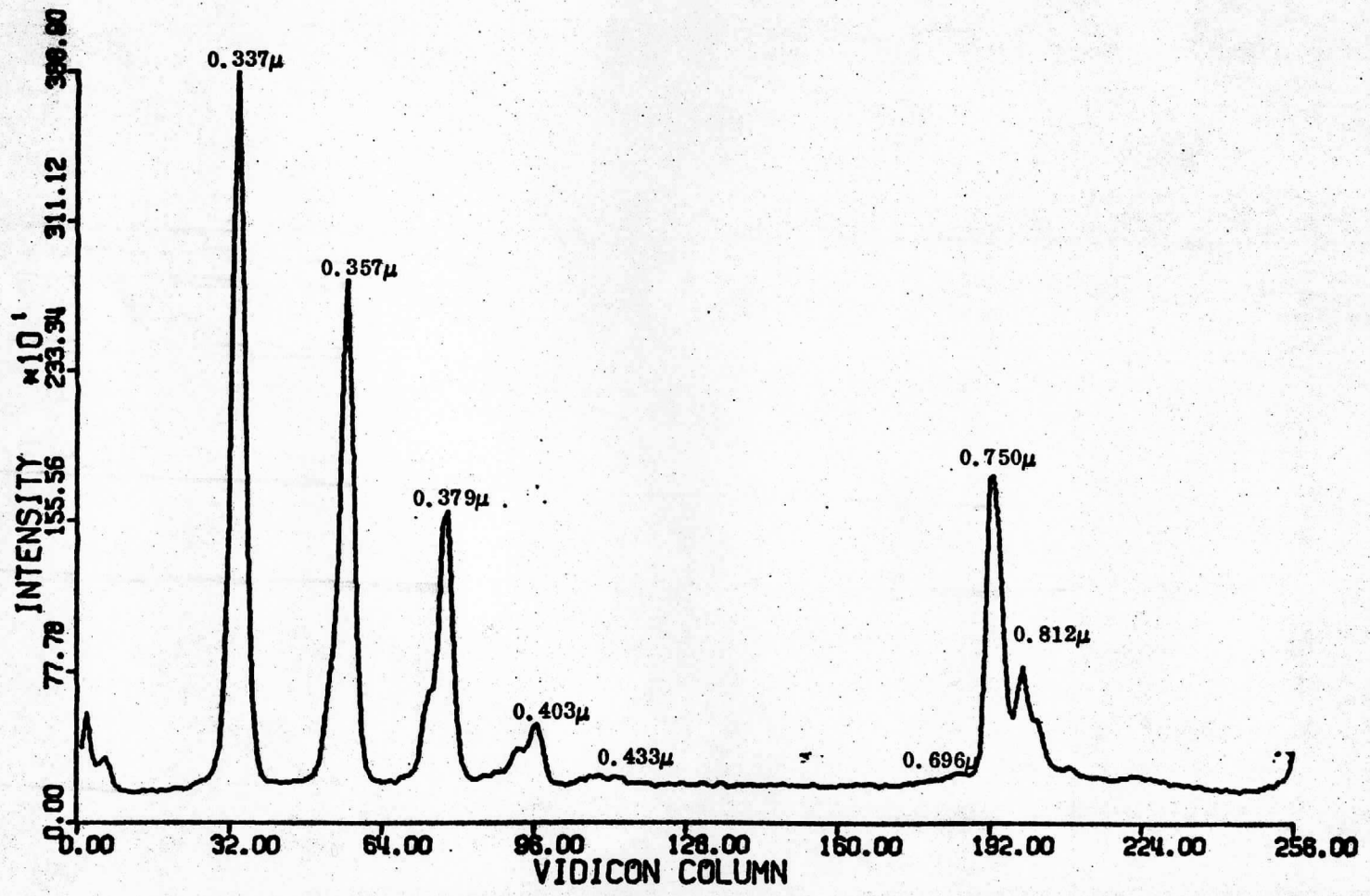


Figure 6. A spectrum of the calibration source, indicating vidicon intensity of each vidicon element along one row. Assigned wavelengths are indicated.

VIDCO2 F.125

S1 = 35.0 L1 = 0.337 S2 = 57.5 L2 = 0.357 S3 = 199.5 L3 = 0.809

LC = 0.1541 C = -41.7388 S0 = -263.2354

1	0.3133	51	0.3508	101	0.4114	151	0.5260	201	0.8248
2	0.3139	52	0.3517	102	0.4130	152	0.5294	202	0.8357
3	0.3145	53	0.3527	103	0.4146	153	0.5328	203	0.8471
4	0.3151	54	0.3536	104	0.4162	154	0.5362	204	0.8588
5	0.3158	55	0.3546	105	0.4179	155	0.5398	205	0.8708
6	0.3164	56	0.3555	106	0.4196	156	0.5433	206	0.8834
7	0.3170	57	0.3565	107	0.4213	157	0.5470	207	0.8963
8	0.3177	58	0.3575	108	0.4230	158	0.5507	208	0.9098
9	0.3183	59	0.3585	109	0.4247	159	0.5546	209	0.9237
10	0.3189	60	0.3595	110	0.4265	160	0.5584	210	0.9382
11	0.3196	61	0.3605	111	0.4283	161	0.5624	211	0.9532
12	0.3203	62	0.3615	112	0.4301	162	0.5664	212	0.9688
13	0.3209	63	0.3626	113	0.4319	163	0.5705	213	0.9850
14	0.3216	64	0.3636	114	0.4338	164	0.5747	214	1.0019
15	0.3223	65	0.3647	115	0.4357	165	0.5790	215	1.0194
16	0.3229	66	0.3657	116	0.4376	166	0.5834	216	1.0378
17	0.3236	67	0.3668	117	0.4395	167	0.5878	217	1.0569
18	0.3243	68	0.3679	118	0.4415	168	0.5924	218	1.0768
19	0.3250	69	0.3690	119	0.4435	169	0.5970	219	1.0977
20	0.3257	70	0.3701	120	0.4455	170	0.6018	220	1.1195
21	0.3264	71	0.3712	121	0.4476	171	0.6066	221	1.1424
22	0.3271	72	0.3724	122	0.4497	172	0.6116	222	1.1663
23	0.3279	73	0.3735	123	0.4518	173	0.6167	223	1.1915
24	0.3286	74	0.3747	124	0.4539	174	0.6219	224	1.2179
25	0.3293	75	0.3759	125	0.4561	175	0.6272	225	1.2458
26	0.3301	76	0.3770	126	0.4583	176	0.6326	226	1.2751
27	0.3308	77	0.3792	127	0.4605	177	0.6381	227	1.3060
28	0.3316	78	0.3795	128	0.4628	178	0.6438	228	1.3387
29	0.3323	79	0.3607	129	0.4651	179	0.6496	229	1.3733
30	0.3331	80	0.3619	130	0.4674	180	0.6556	230	1.4100
31	0.3349	81	0.3832	131	0.4698	181	0.6617	231	1.4489
32	0.3346	82	0.3844	132	0.4722	182	0.6679	232	1.4904
33	0.3354	83	0.3857	133	0.4746	183	0.6743	233	1.5346
34	0.3362	84	0.3870	134	0.4771	184	0.6809	234	1.5818
35	0.3370	85	0.3883	135	0.4796	185	0.6876	235	1.6324
36	0.3378	86	0.3896	136	0.4822	186	0.6945	236	1.6866
37	0.3346	87	0.3910	137	0.4848	187	0.7016	237	1.7451
38	0.3374	88	0.3923	138	0.4874	188	0.7089	238	1.8081
39	0.3403	89	0.3937	139	0.4901	189	0.7164	239	1.8764
40	0.3411	90	0.3951	140	0.4928	190	0.7241	240	1.9505
41	0.3419	91	0.3965	141	0.4956	191	0.7319	241	2.0313
42	0.3428	92	0.3979	142	0.4984	192	0.7401	242	2.1197
43	0.3436	93	0.3993	143	0.5013	193	0.7484	243	2.2168
44	0.3445	94	0.4008	144	0.5042	194	0.7570	244	2.3240
45	0.3454	95	0.4022	145	0.5071	195	0.7658	245	2.4430
46	0.3463	96	0.4037	146	0.5101	196	0.7749	246	2.5758
47	0.3471	97	0.4052	147	0.5132	197	0.7843	247	2.7250
48	0.3480	98	0.4067	148	0.5163	198	0.7939	248	2.8937
49	0.3490	99	0.4083	149	0.5195	199	0.8039	249	3.0862
50	0.3499	100	0.4098	150	0.5227	200	0.8142	250	3.3077

Figure 7. Wavelength as a function of vidicon column for a typical calibration function. The three column(Sn)-wavelength(Ln) pairs used to determine the function are given at the top. Column number is at the left, wavelength at right.

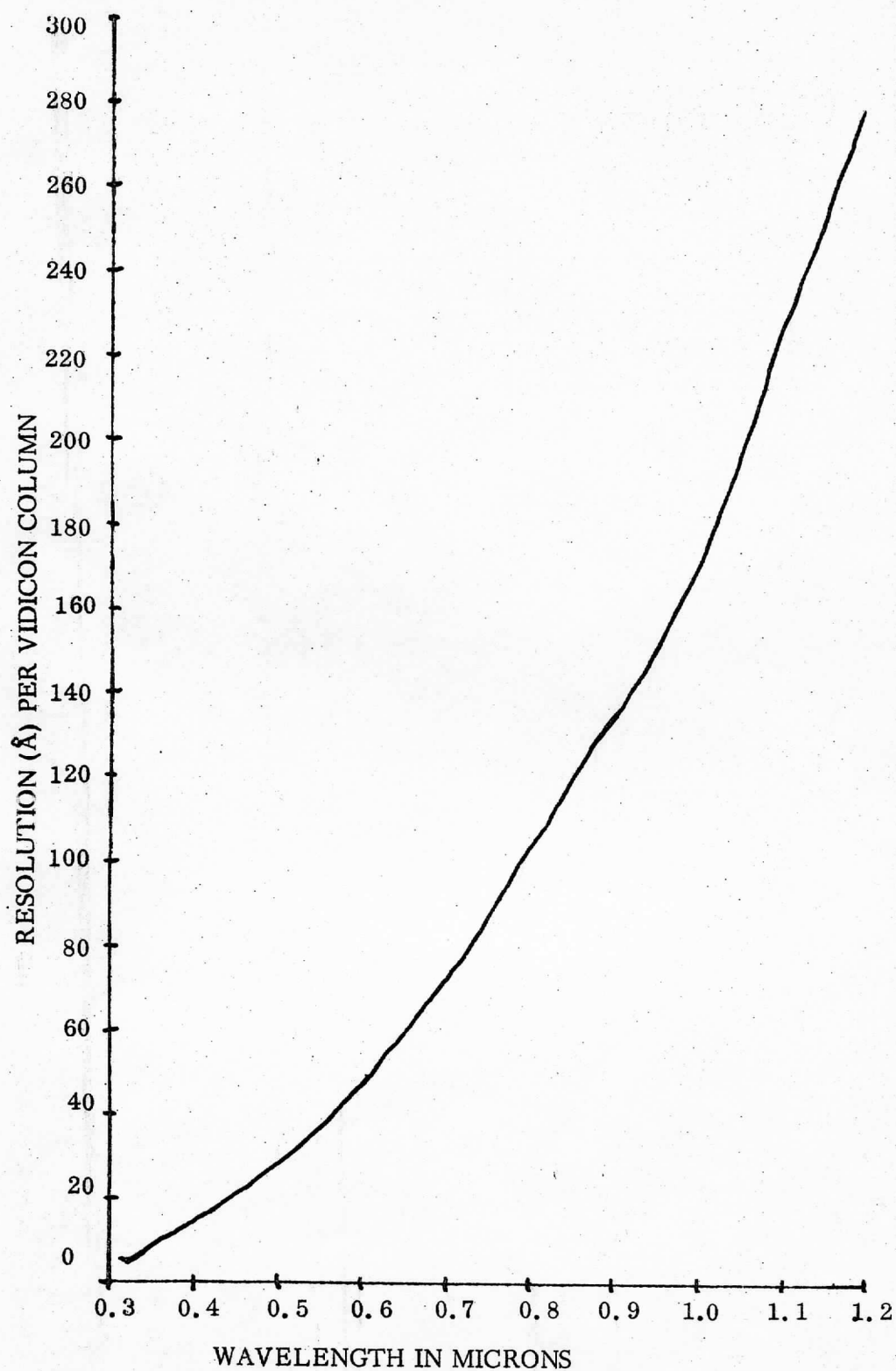


Figure 8. Spectrometer dispersion function.
spectral resolution per image element
as a function of wavelength.

has been written which runs as a subroutine under the Planetary Astronomy Laboratory's image processing system (DIPSY) which has been set up to provide a metastructure under which vidicon images may be easily processed. A simplified diagram of this program appears in Figure 9. The spectral image is read off the run tape by DIPSY and stored on a disk where it is available to the spectral processing routine, which has three basic tasks. The first and easiest is to punch out the intensities along one row of the image onto computer cards for input into a plotting routine (this was how Figure 6 was produced). Second, it can subtract the average background from the image, column by column, where the rows over which the background is to be averaged are read from the input instruction cards. Last, and most important, the program can produce a new image in which all of the elements have the same spectral resolution. For spectral reflectivity work, where the range of interest is 0.4 to 1.2 microns, a resolution of 250 angstroms, the best resolution at 1.2 microns, was chosen. Figures 10 and 11 show the effects of this processing on an image of the standard star Xi 2 Ceti. Portions of these images are then integrated spatially along the slit. Due to atmospheric and telescope optical effects, a star image is not a point; it is smeared out spatially into a Gaussian distribution of intensity which is at its maximum where the point source would be. To use the full energy output of the star at a given wavelength, the image must be integrated across all rows where the image intensity is

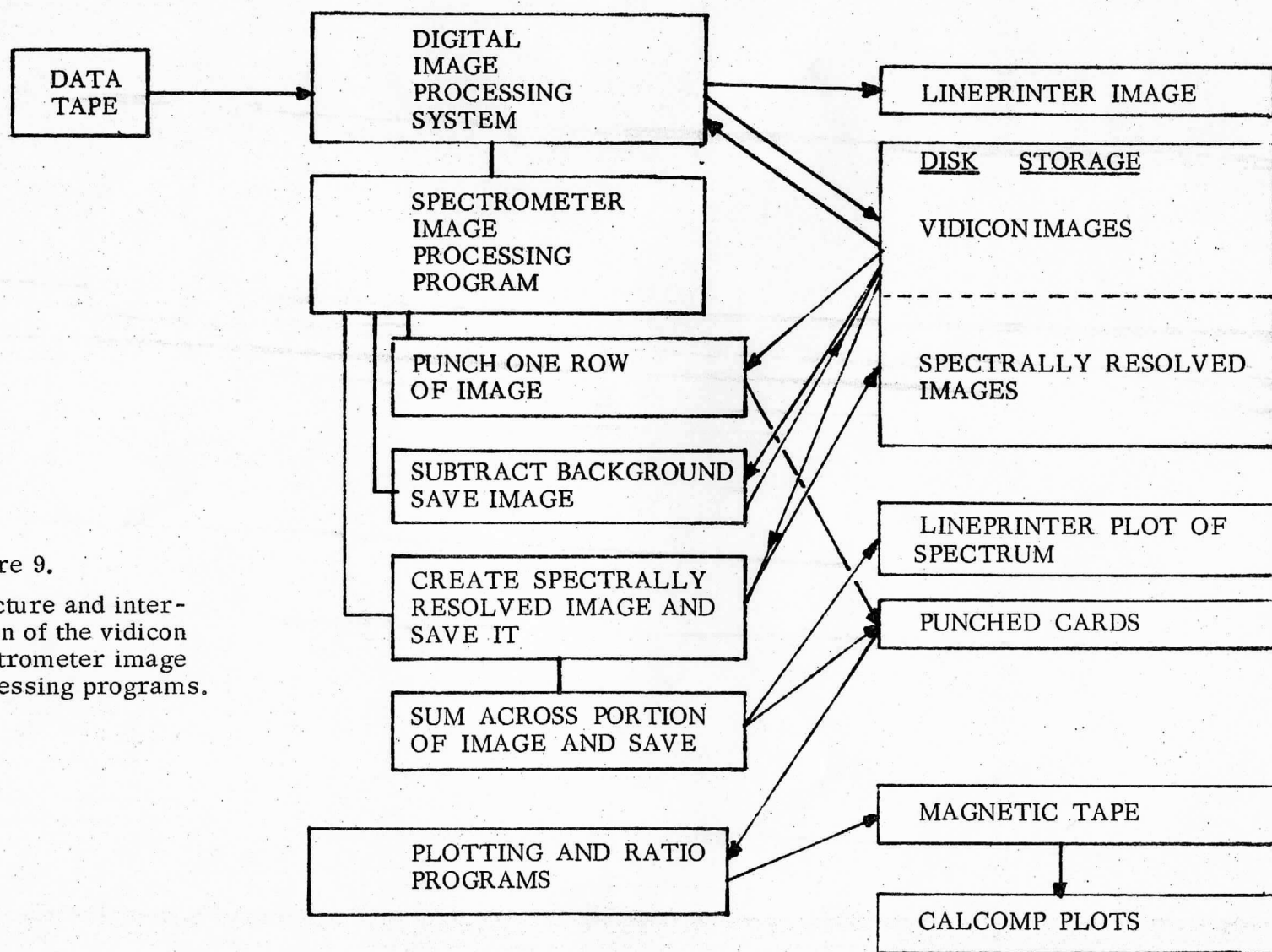


Figure 9.

Structure and interaction of the vidicon spectrometer image processing programs.

151		152		153		154		155		156		157		158		159		160		161		162		163		164		165		166		167		168		169		170		171		172		173		174		175	
1-		440		437		436		437		441		442		443		436		446		450		448		454		447		443		449		440		427		412		335		411		411		336		447			
2-		204		206		112		212		179		195		195		191		196		193		191		195		194		199		192		199		231		131		135		127		133		149		128			
3-		155		160		120		155		167		167		167		167		163		163		163		162		166		161		160		159		160		157		164		153		172							
4-		136		164		154		149		152		139		149		151		152		153		144		145		151		145		140		141		145		153		149											
5-		148		165		165		167		167		145		146		161		143		144		144		140		141		147		145		142		145		141		143											
6-		135		135		141		160		157		145		144		133		134		141		138		135		141		144		144		131		135		142													
7-		137		152		145		139		144		147		160		137		157		146		144		143		145		142		134		147		133		133													
8-		162		134		126		133		127		125		136		139		137		131		123		131		135		127		143		131		131															
9-		135		161		131		135		138		131		132		129		141		143		132		139		135		141		141		125		137		131													
10-		127		149		143		127		133		135		129		132		137		131		145		135		126		133		132		143		142															
11-		132		126		127		177		127		130		127		134		130		136		141		135		127		135		140		140		135		127													
12-		133		132		127		137		141		162		135		132		143		136		129		136		122		124		132		135		135															
13-		135		134		127		131		139		142		141		144		147		137		134		143		131		136		141		137		135															
14-		132		133		141		137		135		127		127		129		137		133		132		124		129		133		131		125		125															
15-		127		131		138		137		135		132		132		127		127		136		133		131		129		125		132		137		137															
16-		137		136		133		128		131		130		127		139		134		131		134		131		132		126		124		137		137															
17-		126		127		127		137		139		129		127		135		124		125		137		131		139		127		127		137		137															
18-		178		183		171		179		165		177		178		172		179		180		175		186		179		173		172		177		171		180													
19-		147		154		163		163		131		135		135		141		142		141		145		127		136		139		136		131		135		144													
20-		143		131		133		137		134		135		127		129		129		140		135																											

SX20711n	1	2	3	4	5	6	7	8	9	10	11	12	13	14					
1-	375.5	419.2	3	401.2	28	524.7	4	519.9	21	505.111	502.544	495.473	274.796	511.365	493.337	491.379	487.122	467.32	
2-	60.476	71.571	11.715	128.548	35.361	91.448	99.429	134.028	96.912	95.749	93.933	94.580	73.417	57.55					
3-	17.263	20.064	41.524	42.077	22.481	25.562	28.97	27.992	41.769	41.238	4.257	33.163	17.599	11.427					
4-	7.6	7.725	16.848	17.724	16.121	12.199	11.460	9.442	17.813	14.103	10.804	5.642	0.743	5.62					
5-	2.245	9.883	11.325	6.721	7.6	6.007	4.117	5.542	11.451	6.826	6.476	3.216	0.005	5.62					
6-	12.997	8.571	11.3	2.432	2.617	3.534	3.976	2.947	4.399	6.737	6.978	0.000	0.000	0.00					
7-	0.242	7.272	1.272	0.87	1.463	3.595	4.555	7.326	11.514	1.324	4.046	0.206	0.000	0.00					
8-	6.713	4.364	3.924	3.638	2.576	2.363	1.295	4.269	0.372	0.967	1.692	0.198	0.000	0.00					
9-	3.117	8.649	3.873	1.24	1.558	2.232	1.478	2.112	1.363	2.714	1.844	0.028	0.233	0.00					
10-	6.199	2.323	0.225	1.45	2.627	1.040	1.72	4.967	6.620	2.242	0.00	0.010	0.017	0.00					
11-	2.943	3.824	1.646	1.518	3.669	0.579	0.560	0.000	0.196	0.224	0.00	0.000	0.010	0.00					
12-	3.583	5.711	1.094	0.215	0.712	0.634	2.020	1.166	4.399	0.578	0.243	0.000	0.000	0.00					
13-	4.447	1.683	0.262	1.27	0.000	0.000	2.167	2.451	5.277	6.147	1.349	0.000	0.010	0.00					
14-	3.407	3.367	0.115	0.965	4.204	6.337	3.425	2.332	1.446	0.153	0.000	0.000	0.000	0.00					
15-	3.298	3.665	0.469	0.347	0.375	0.496	0.009	0.100	0.620	0.260	0.000	0.000	0.000	0.00					
16-	3.891	4.378	0.000	0.543	0.000	0.696	1.644	1.597	1.373	1.180	5.106	0.227	0.070	0.18					
17-	1.303	1.201	0.015	0.812	1.342	0.634	1.249	0.000	0.134	0.024	0.000	0.000	0.000	0.00					
18-	1.204	0.266	0.404	0.018	0.000	0.193	0.184	0.207	0.437	0.000	0.000	0.000	0.000	0.00					
19-	5.103	2.435	0.087	0.832	0.928	1.336	0.514	0.000	0.000	1.439	2.175	0.000	0.000	0.03					
20-	0.767	1.667	0.000	0.728	1.088	1.756	1.246	0.734	0.000	0.024	0.000	0.000	0.000	0.00					
21-	1.936	2.015	0.010	1.634	0.603	1.165	0.735	0.184	1.075	0.177	0.513	0.000	0.000	0.00					
22-	4.513	3.171	0.000	0.335	0.019	0.103	0.618	0.734	3.515	2.112	0.823	0.000	0.000	0.00					
23-	1.276	1.764	0.302	1.165	2.309	2.507	1.809	1.432	1.952	2.903	0.000	0.000	0.000	0.00					
24-	1.4	1.71	0.000	0.431	0.579	0.165	0.009	0.918	1.033	0.236	0.275	0.000	0.000	0.00					
25-	5.144	3.341	0.019	0.344	0.229	0.138	1.065	0.184	0.826	0.000	0.000	0.000	0.000	0.00					
26-	1.223	0.611	0.018	0.209	0.083	0.675	0.000	1.799	0.413	0.024	0.000	0.000	0.000	0.00					
27-	1.107	3.706	0.023	2.272	0.725	0.324	0.569	1.74	1.776	2.584	2.202	0.000	0.020	0.00					
28-	1.020	2.750	0.007	0.777	1.782	0.303	0.009	0.991	3.129	1.333	0.513	0.000	0.050	0.00					
29-	0.172	0.556	0.000	5.380	4.572	0.169	15.500	13.119	9.283	4.826	1.569	0.000	0.000	0.00					
30-	1.750	1.060	11.719	49.466	78.571	95.956	108.560	126.612	126.445	111.197	63.749	62.049	46.657	31.221					
31-	4.913	13.903	11.653	31.847	551.710	720.357	815.295	935.781	929.618	891.125	754.278	667.237	555.143	57.429					
32-	5.844	35.645	49.089	1291.697	1451.6	2393.964	263.129	2925.239	2944.294	2844.202	2659.112	2494.456	2274.702	1924.473					
33-	5.994	53.675	611.482	275.742	3.15.479	366.561	4056.195	4466.492	4562.047	4464.301	4364.478	3648.593	3418.515	3245.478					
34-	5.839	51.007	44.651	1125.650	1617.617	2269.134	2976.136	2616.558	2624.630	2717.977	2466.240	2310.043	2036.648	1859.471					
35-	4.874	22.457	21.675	64.463	631.661	787.384	9.2.716	1.16.936	1.4.7.5	111.7.312	111.9.8	1.84.446	1713.769	974.53					
36-	2.429	12.817	110.321	271.257	70.051	357.981	393.263	442.41	491.991	92.346	536.829	510.613	507.491	477.492					
37-	1.108	5.137	41.443	46.105	118.508	141.033	156.197	175.017	197.282	27.639	710.644	236.009	186.634	174.572					
38-	2.925	3.499	7.103	18.375	37.361	5.772	56.637	56.452	64.694	57.668	35.947	5.5.1	29.816	51.550					
39-	1.256	1.953	0.594	5.634	16.757	11.751	16.762	15.576	2.809	2.269	0.000	0.010	0.000	0.000					
40-	1.744	4.484	1.006	0.397	1.107	0.992	0.002	1.647	0.960	0.201	0.000	0.000	0.066	0.017					
41-	1.897	1.003	0.037	0.253	0.426	0.214	0.147	0.312	0.000	0.614	0.000	0.000	0.017	0.083					
42-	0.431	1.157	0.4	2.536	1.360	0.000	0.018	0.000	0.000	0.000	0.00	0.00	0.000	0.000					
43-	1.631	4.140	1.525	0.022	0.630	0.344	0.156	0.000	2.013	1.133	0.000	0.303	0.311						
44-	2.139	3.205	0.646	1.066	0.009	0.765	0.009	0.129	0.000	0.389	0.000	0.000	0.000	0.196					
45-	0.550	2.496	1.75	0.419	0.445	1.619	1.221	0.514	0.764	1.007	0.000	0.026	0.033	0.066					
46-	1.651	1.945	1.957	0.812	1.119	1.124	0.376	0.035	0.000	0.000	1.349	0.028	0.033	1.126					
47-	2.893	1.533	0.528	0.050	1.300	0.689	0.707	2.451	0.000	0.024	0.828	1.32	2.317	1.122					
48-	1.808	0.773	1.629	2.447	1.984	3.051	0.569	0.863	1.027	1.428	0.215	2.02	0.011	0.162					
49-	1.365	4.118	4.551	0.656	0.013	0.455	0.000	0.000	1.232	0.000	1.927	0.000	0.396	4.093					
50-	3.575	3.374	1.172	0.610	0.967	0.661	1.074	1.652	0.000	0.024	1.101	0.509	3.401	12.413					
51-	1.693	0.615	1.962	2.084	1.694	0.399	0.551	2.304	0.341	0.000	0.000	0.026	0.083	1.56					
52-	2.512	1.334	7.252	4.305	0.223	1.474	0.000	0.000	0.620	0.319	1.073	1.514	7.673	7.131					
53-	4.267	5.939	3.607	1.698	0.006	0.758	0.039	0.707	1.033	1.605	3.124	13.072	12.646	7.131					
54-	3.827	1.205	3.517	4.496	1.688	0.716	2.671	1.477	1.144	3.000	4.7.9	1.0.5	1.82						
55-	2.638	2.762	1.399	9.018	1.787	0.124	0.000	0.367	0.000	1.581	8.327	10.320	9.344	1.181					
56-	1.797	1.622	3.212	1.005	0.343	0.716	0.018	0.679	0.000	2.936	5.395	13.027	9.014	1.774					

Figure 11. A portion of the processed image of ξ^2 Ceti from 0.35μ to 0.70μ . Each image element represents intensity per ten angstroms averaged over a 250 angstrom resolution element. The background was first subtracted out of the vidicon image.

Spectrum	1	2	3	4	5	6	7	8	9	10	11	12	13	14
1-	375.5	419.2	430.2	431.2	432.2	433.2	434.2	435.2	436.2	437.2	438.2	439.2	440.2	441.2
2-	60.476	71.571	71.715	128.548	95.361	91.448	99.429	104.028	96.912	95.749	93.933	94.580	73.417	57.552
3-	17.263	20.064	41.524	42.077	22.481	25.562	28.97	27.992	41.769	41.238	4.257	33.163	17.599	11.427
4-	7.6	7.725	16.848	17.724	16.121	12.199	11.460	9.142	17.813	14.100	10.804	5.642	0.743	0.523
5-	2.245	9.883	11.375	6.721	7.67	6.007	4.117	5.534	3.976	2.947	4.399	6.737	6.978	0.000
6-	12.997	8.471	11.373	2.432	2.617	3.534	3.976	4.555	7.326	11.514	1.324	4.046	0.206	0.000
7-	0.242	7.272	1.272	0.87	1.463	3.595	4.555	7.326	11.514	1.324	4.046	0.206	0.000	0.00
8-	6.713	4.364	3.924	3.638	2.576	2.363	1.295	4.269	0.372	0.967	1.899	0.198	0.000	0.00
9-	3.117	8.649	3.873	1.24	1.558	2.232	1.478	2.112	1.363	2.714	1.844	0.028	0.233	0.00
10-	6.199	2.323	0.225	1.45	2.627	1.040	1.72	4.967	0.620	2.242	0.00	0.010	0.010	0.00
11-	2.943	3.874	1.646	1.518	3.669	0.579	0.560	0.000	0.196	0.224	0.00	0.000	0.010	0.00
12-	3.583	5.711	1.094	0.215	0.712	0.634	2.020	1.166	4.399	0.578	0.243	0.000	0.000	0.00
13-	4.447	1.683	0.262	1.27	0.000	0.000	2.167	2.451	5.277	6.147	1.349	0.000	0.000	0.00
14-	3.407	3.367	0.115	0.965	4.204	6.337	3.425	2.332	1.446	0.153	0.000	0.000	0.000	0.00
15-	3.298	3.065	0.469	0.347	0.375	0.496	0.009	0.100	0.620	0.260	0.000	0.000	0.000	0.00
16-	3.891	4.378	0.000	0.543	0.000	0.696	1.044	1.597	1.373	1.180	5.106	0.227	0.030	0.05
17-	1.303	1.201	0.015	0.812	1.342	0.634	1.249	0.000	0.134	0.024	0.000	0.000	0.000	0.00
18-	1.204	0.266	0.404	0.018	0.000	0.193	0.184	0.207	0.437	0.000	0.000	0.000	0.000	0.00
19-	5.103	2.435	0.087	0.832	0.928	1.336	0.514	0.000	0.000	1.439	2.175	0.000	0.000	0.03
20-	0.767	1.667	0.000	0.728	1.088	1.756	1.246	0.734	0.000	0.024	0.000	0.000	0.000	0.00
21-	1.936	2.015	0.010	1.314	0.063	1.165	0.735	0.184	1.075	0.177	0.513	0.000	0.000	0.00
22-	4.513	3.171	0.000	0.335	0.019	0.103	0.818	0.734	3.515	2.112	0.823	0.000	0.000	0.00
23-	1.276	1.764	0.302	1.165	2.309	2.507	1.809	1.432	1.952	2.903	0.000	0.000	0.000	0.00
24-	1.449	1.71	0.000	0.431	0.579	0.165	0.009	0.018	1.033	0.236	0.275	0.000	0.000	0.00
25-	5.144	3.341	0.019	0.344	0.229	0.138	1.065	0.184	0.826	0.000	0.000	0.000	0.000	0.00
26-	1.223	0.611	0.018	0.209	0.083	0.675	0.000	1.799	0.413	0.024	0.000	0.000	0.000	0.00
27-	1.102	3.706	0.023	2.272	0.725	0.324	0.569	1.774	1.776	2.584	2.202	0.000	0.000	0.00
28-	1.020	2.150	0.007	0.777	1.782	0.303	0.009	0.991	3.129	1.333	0.513	0.000	0.050	0.00
29-	0.172	0.556	0.000	5.380	4.572	0.169	15.500	13.119	9.283	4.826	1.569	0.000	0.000	0.06
30-	1.750	1.060	11.719	49.486	78.571	95.956	108.560	126.612	126.445	111.197	63.749	62.009	46.657	31.221
31-	4.973	13.903	116.553	311.847	551.710	726.357	815.295	935.781	929.618	691.125	754.278	667.237	555.143	47.429
32-	5.843	35.645	49.600	1291.697	1451.6	2393.964	263.129	2925.239	2464.294	2845.202	2659.112	2495.456	2275.702	1975.173
33-	5.994	53.675	111.482	225.742	315.479	360.541	405.195	4466.492	4562.047	4464.301	4264.478	3664.843	3418.515	3245.478
34-	5.839	51.007	44.651	1125.650	1617.617	2269.134	2976.136	2616.556	2624.630	2717.977	2466.240	2310.043	2036.648	1859.417
35-	4.874	22.457	21.675	464.673	631.661	787.384	9.2716	1.69.936	1.4	1.7	1.5	111.732	111.948	1.84.446
36-	2.429	12.817	110.321	271.257	400.051	357.981	393.263	442.41	491.991	524.346	536.829	507.633	507.491	477.492
37-	1.108	5.137	41.443	94.105	118.508	141.033	156.197	175.017	197.732	217.639	210.644	216.809	186.634	174.572
38-	2.925	3.499	7.103	18.375	37.361	51.772	56.637	56.452	64.694	57.668	55.947	5	29.816	31.550
39-	1.256	1.953	0.594	5.634	16.757	11.751	16.762	15.576	2.809	2.289	0.000	0.000	0.000	0.000
40-	1.754	4.494	1.006	0.397	1.107	0.992	0.009	1.047	0.960	0.201	0.000	0.000	0.066	0.017
41-	1.897	1.003	0.037	0.253	0.426	0.214	0.147	0.312	0.000	0.614	0.000	0.000	0.017	0.083
42-	0.431	1.157	0.44	2.536	1.360	0.000	0.018	0.000	0.000	0.000	0.000	0.000	0.000	0.000
43-	1.631	4.140	1.525	0.022	0.630	0.344	0.156	0.000	2.013	1.133	0.000	0.303	0.311	0.000
44-	2.139	3.203	0.646	1.066	0.009	0.765	0.009	0.129	0.000	0.389	0.000	0.000	0.000	0.196
45-	0.550	2.496	1.75	0.419	0.445	1.619	1.221	0.514	0.164	1.007	0.000	0.126	0.033	0.066
46-	1.551	1.945	1.957	0.812	1.119	1.124	0.376	0.035	0.000	1.349	0.028	0.033	1.126	0.000
47-	2.893	1.133	0.528	0.050	1.300	0.689	0.707	2.451	0.000	0.024	0.828	1.	2.317	1.172
48-	1.808	0.773	1.629	2.447	1.984	3.051	0.569	0.863	1.027	1.428	0.215	2.02	0.011	0.162
49-	1.365	4.118	4.551	0.656	0.013	0.455	0.000	0.000	1.232	0.000	1.927	0.000	0.396	4.093
50-	3.575	3.374	1.172	0.610	0.967	0.661	1.074	1.652	0.000	0.024	1.101	0.509	3.401	12.413
51-	1.693	0.615	1.962	2.084	1.694	0.399	0.551	2.304	0.341	0.000	0.026	0.083	1.	56
52-	2.512	1.334	7.252	4.305	0.223	1.474	0.000	0.000	0.620	0.319	1.073	1.514	7.693	7.131
53-	4.267	5.929	3.607	1.698	0.006	0.758	0.059	0.707	1.033	1.605	3.124	13.072	12.646	7.131
54-	3.827	1.205	6.235	3.517	4.496	1.688	0.716	2.671	1.477	1.144	3.000	4.7.9	1.0.5	5.827
55-	2.638	2.762	1.399	9.318	1.787	0.124	0.000	0.367	0.000	1.581	8.327	10.320	9.344	1.181
56-	1.797	1.622	3.212	1.005	0.343	0.716	0.018	0.679	0.000	2.936	5.395	13.027	9.014	1.771

Figure 11. A portion of the processed image of ξ^2 Ceti from 0.35μ to 0.70μ . Each image element represents intensity per ten angstroms averaged over a 250 angstrom resolution element. The background was first subtracted out of the vidicon image.

above the background. After this integration, the spectrum vector is punched out onto cards for plotting and further processing. A more advanced version of this processor will incorporate the plotting, ratioing, and other functions into one DIPSYs subsystem, where only disk files will be used.

The final procedure needed for good spectral reflectivity data of the surface of a planet is to know from what part of the surface the spectrum originates. A photograph is taken through the eyepiece, looking at the slit in a mirror tilted 45 degrees to the optical axis of the telescope (the first surface in Figure 3). A similar logging arrangement is used for photometer data. A plotting program has been written to create Calcomp plots of the coordinate grid of Mars (or any other planet) projected onto a disk using the physical ephemeris of the planet from The American Ephemeris and Nautical Almanac and the time of observation in Universal Time. Figure 12 is a block diagram of the program, while Figure 13 is a typical, although smaller than normal, output. To position the spectrometer slit on the disk of the planet, the negative of the photograph of the telescope image is projected onto the grid, and the slit marked by hand. At this point the original vidicon images have been reduced to constant resolution spectra of stars and known positions on Mars; and reduction to spectral reflectivity data, as well as testing, can begin.

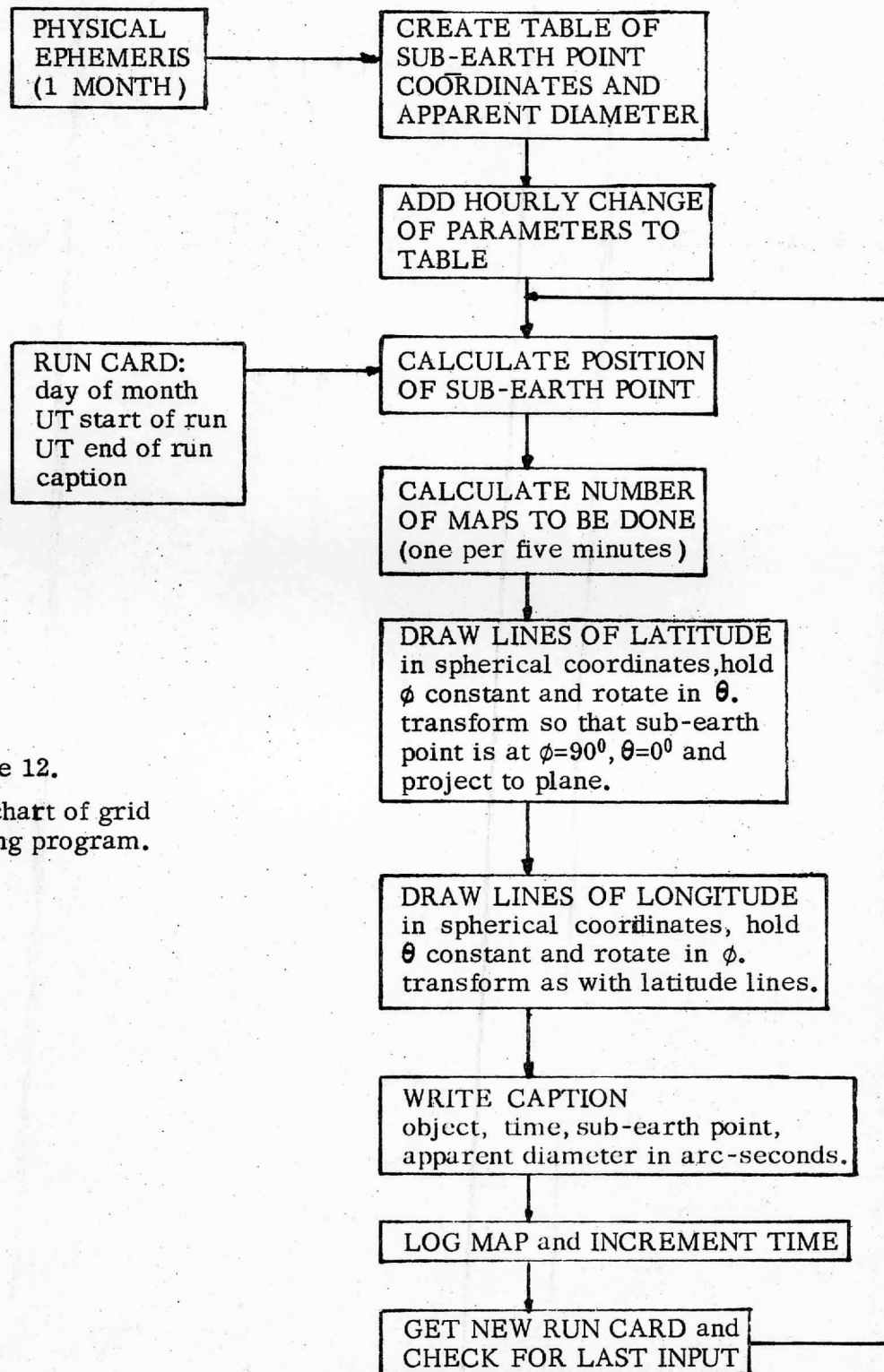
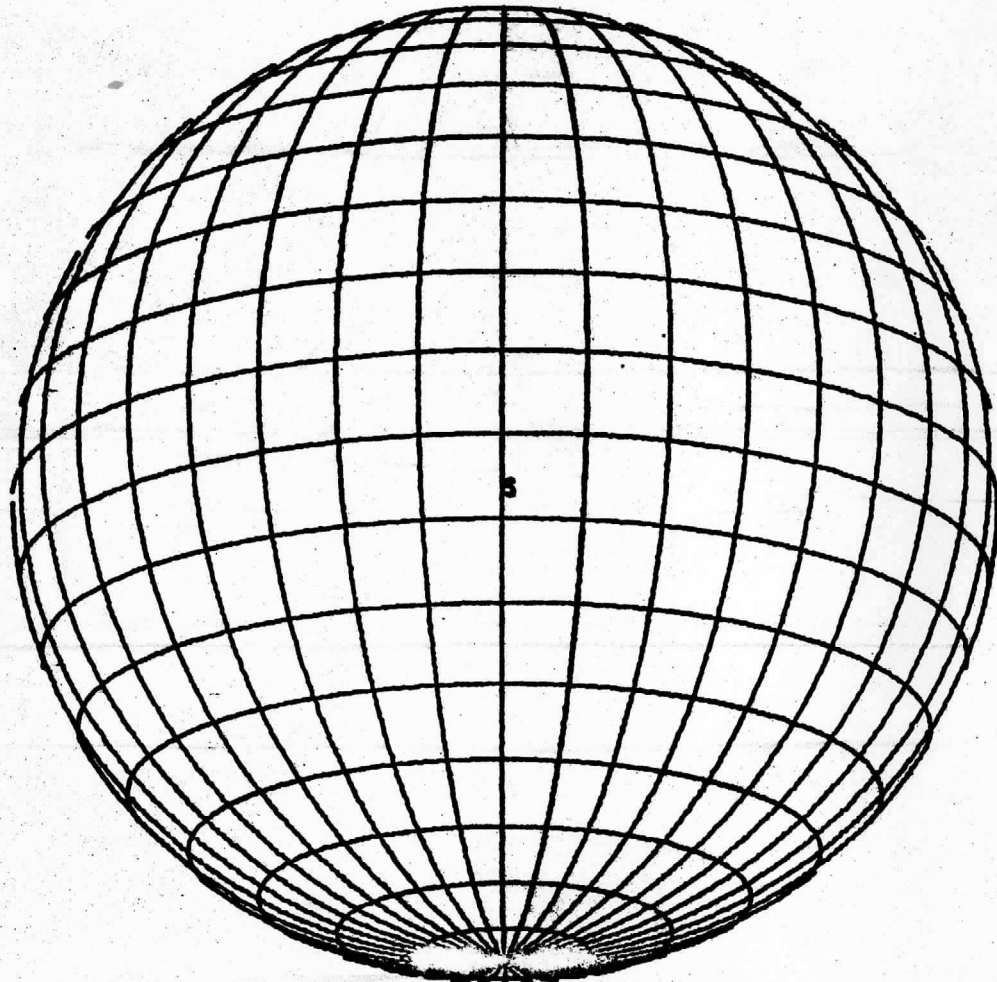


Figure 12.

Flowchart of grid plotting program.



MARS
VIDSPEC C
4 OF 4
OCT. 18, 1973
T = 8:58 UT
LAT = -17.3
LONG = 9.8
DIA = 21.46 SEC

Figure 13. A typical grid plot produced by the program in Figure 12,
the third produced for vidicon spectrometer Mars run C.

IV. Analysis of Data

The first major attempt to use the vidicon spectrometer to take spectra for reflectivity work occurred during the opposition of Mars during October, 1973. On two consecutive nights the Mauna Kea eighty-inch reflector was trained on the planet Mars, and about 75 spectra were taken, as well as an equal number of spectra of the standard stars Alpha Lyra and Xi 2 Ceti. Xi 2 Ceti was chosen because it was near Mars in the sky, while Alpha Lyra has a spectrum which is well known and is used to calculate planet/sun ratios to get reflectivity. Figure 14 demonstrates the reduction methods used to get spectral reflectivities from raw intensity spectra. To avoid airmass reductions, spectra of Alpha Lyra and Xi 2 Ceti were taken when the two stars were at the same airmass, 1.38. Since star/star ratios exhibit little variation with low airmass changes, the ratio of the two stars obtained from these spectra can also be used to reduce reflectivities at other airmasses. Before any data was reduced to reflectivities, extensive testing was done to see whether the data would be usable. This portion of the thesis will describe that work, using the best results obtained to date.

Figure 15 shows a high resolution spectrum of Alpha Lyra which has been averaged over 250 angstrom segments to simulate the spectrometer output. Figure 16 is an Alpha Lyra spectrum from the vidicon spectrometer from which the vidicon response has been

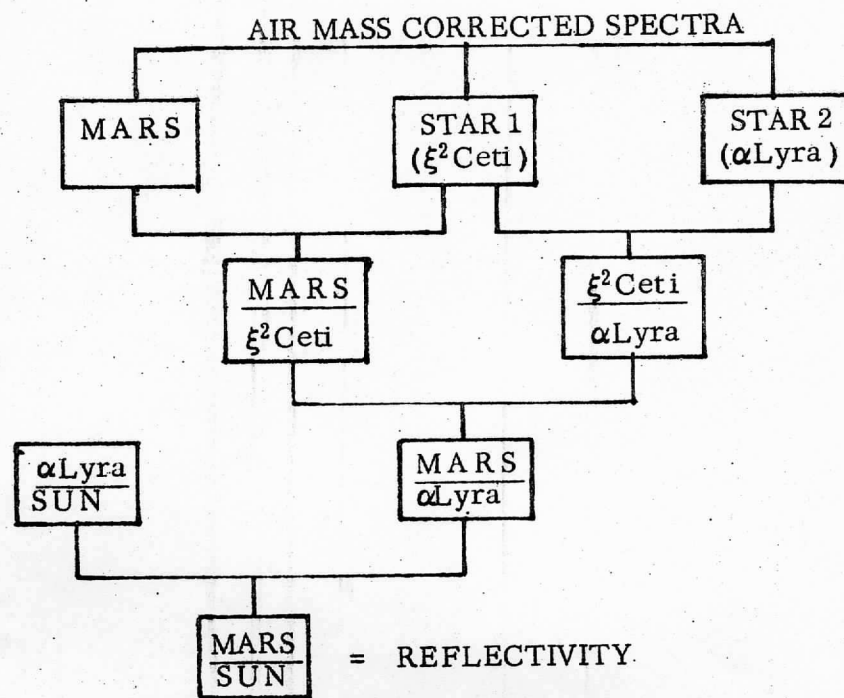


Figure 14. Production of spectral reflectivity from raw spectra. Air mass correction not needed if objects to be ratioed are at the same air mass.

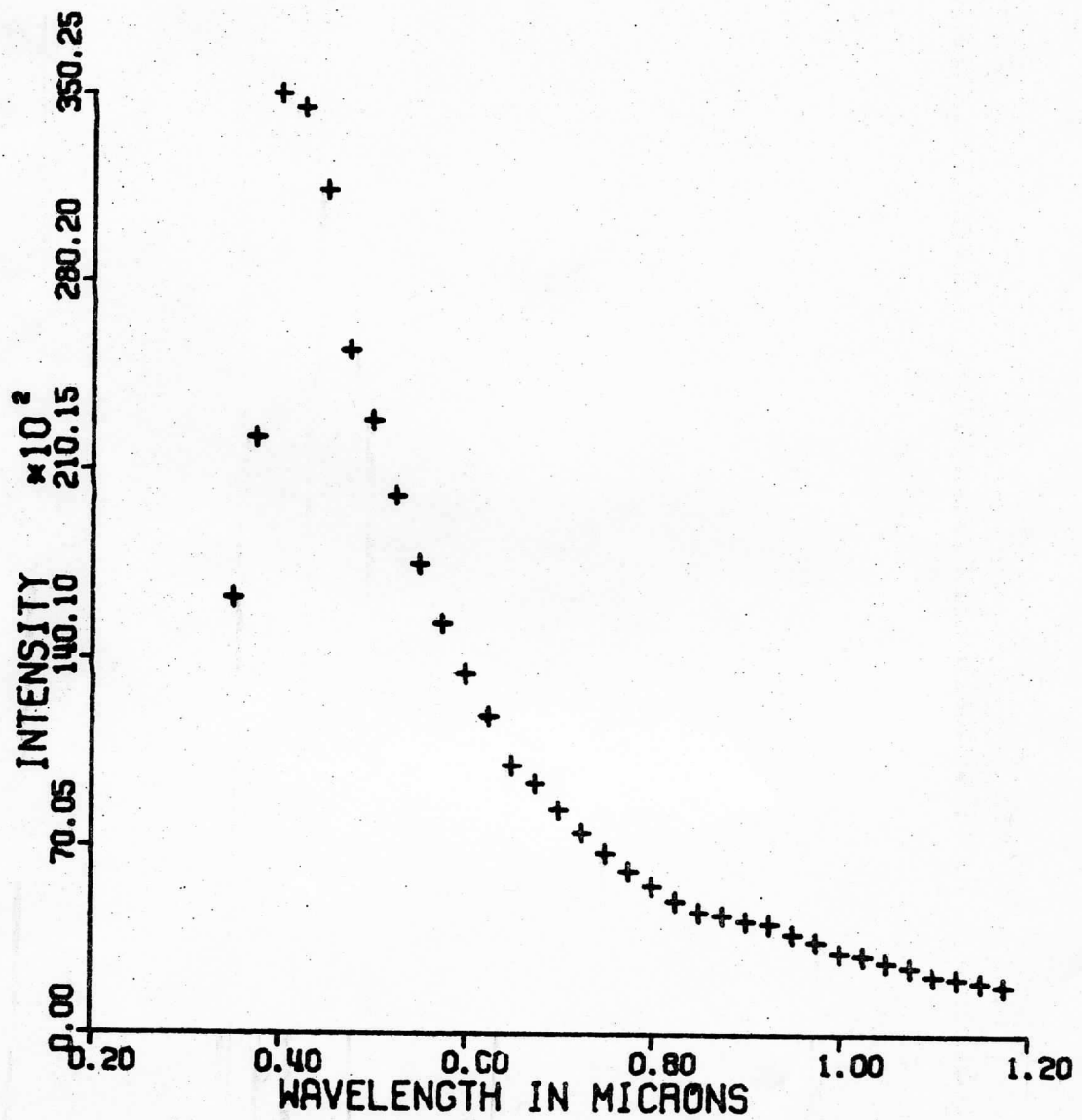
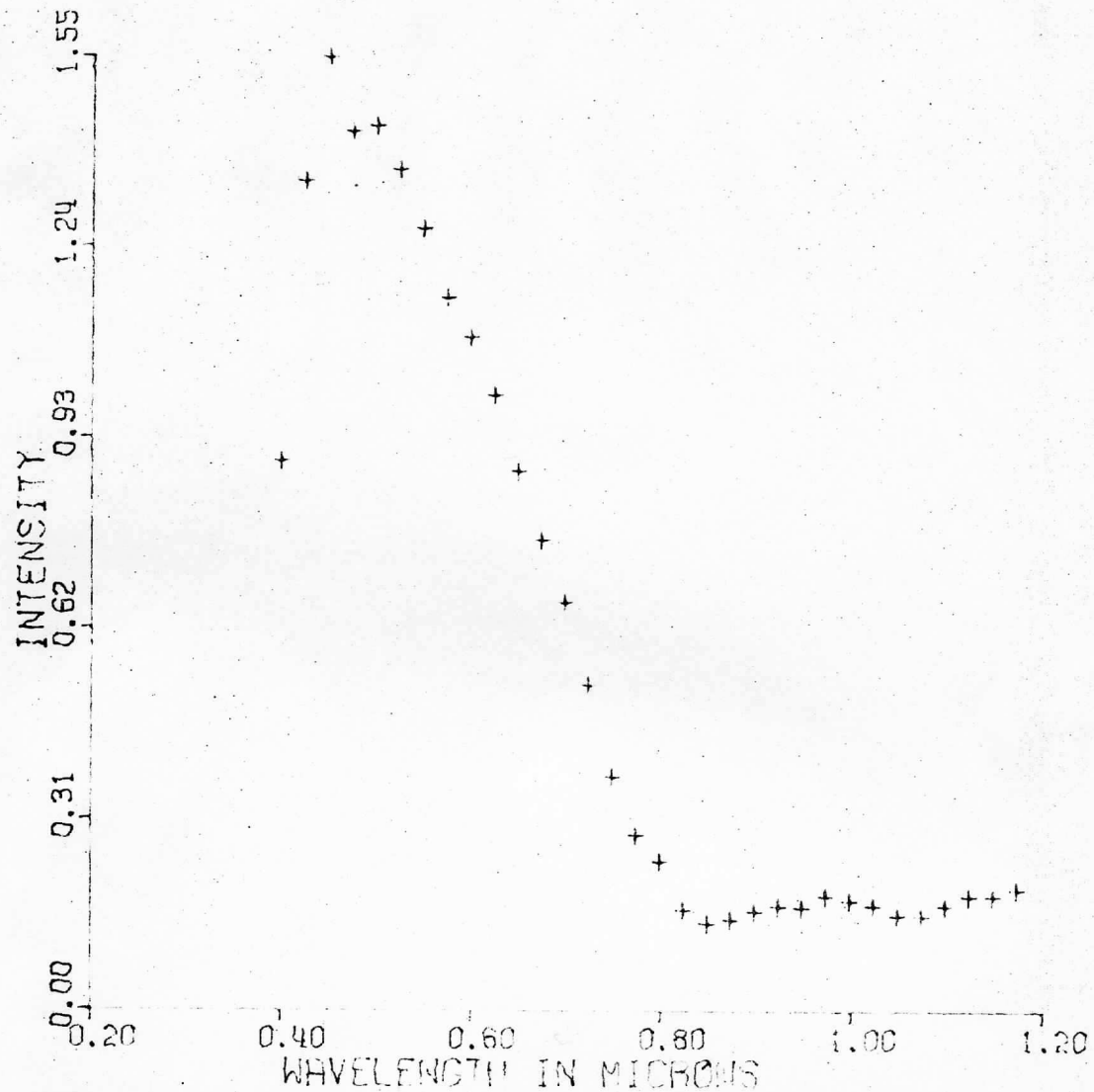


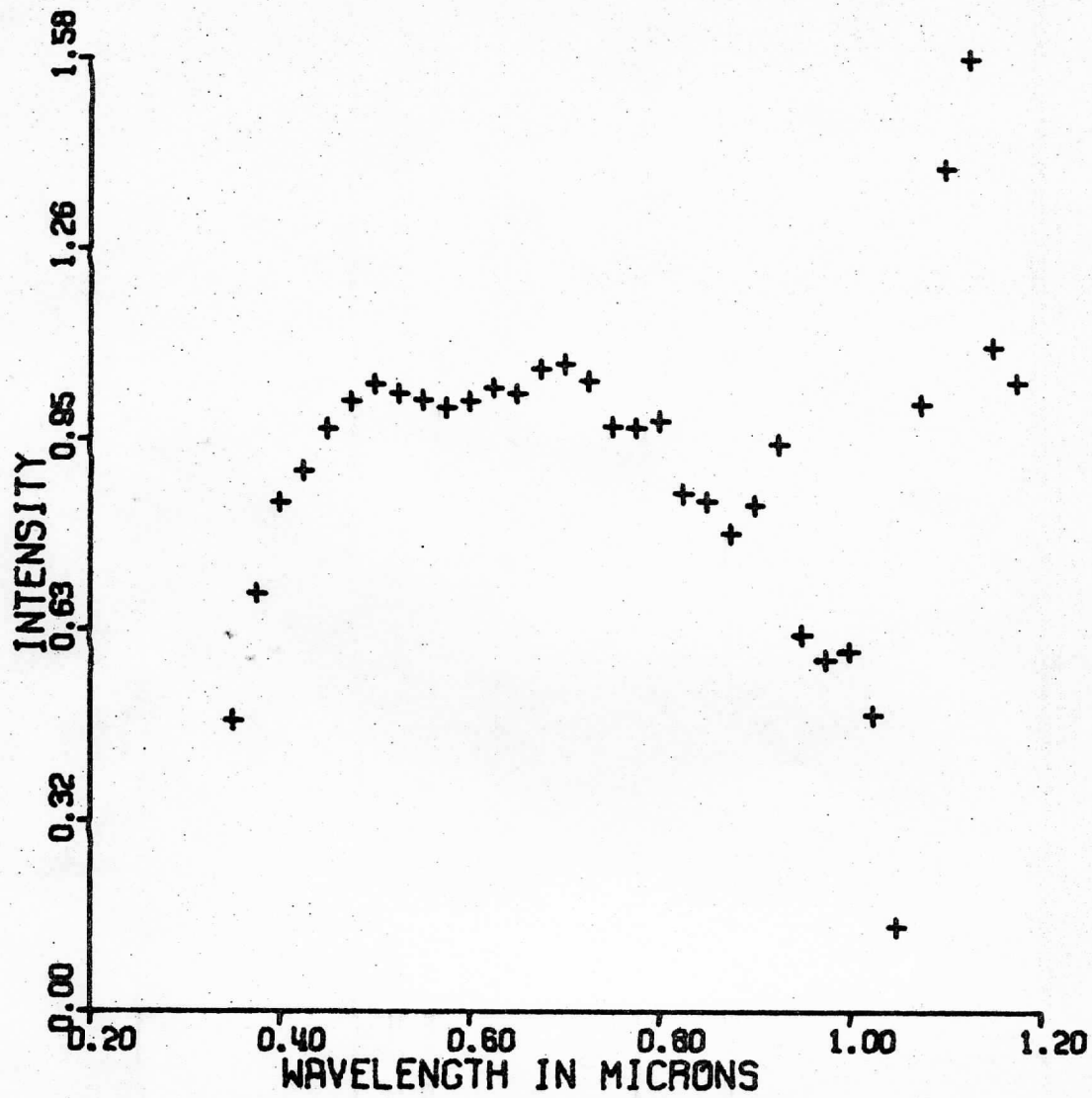
Figure 15. Spectrum of α Lyra, averaged over 250 angstrom resolution elements, from a 50 angstrom resolution spectrum provided by Steve Kent.



SAT YR87 / VIDICON

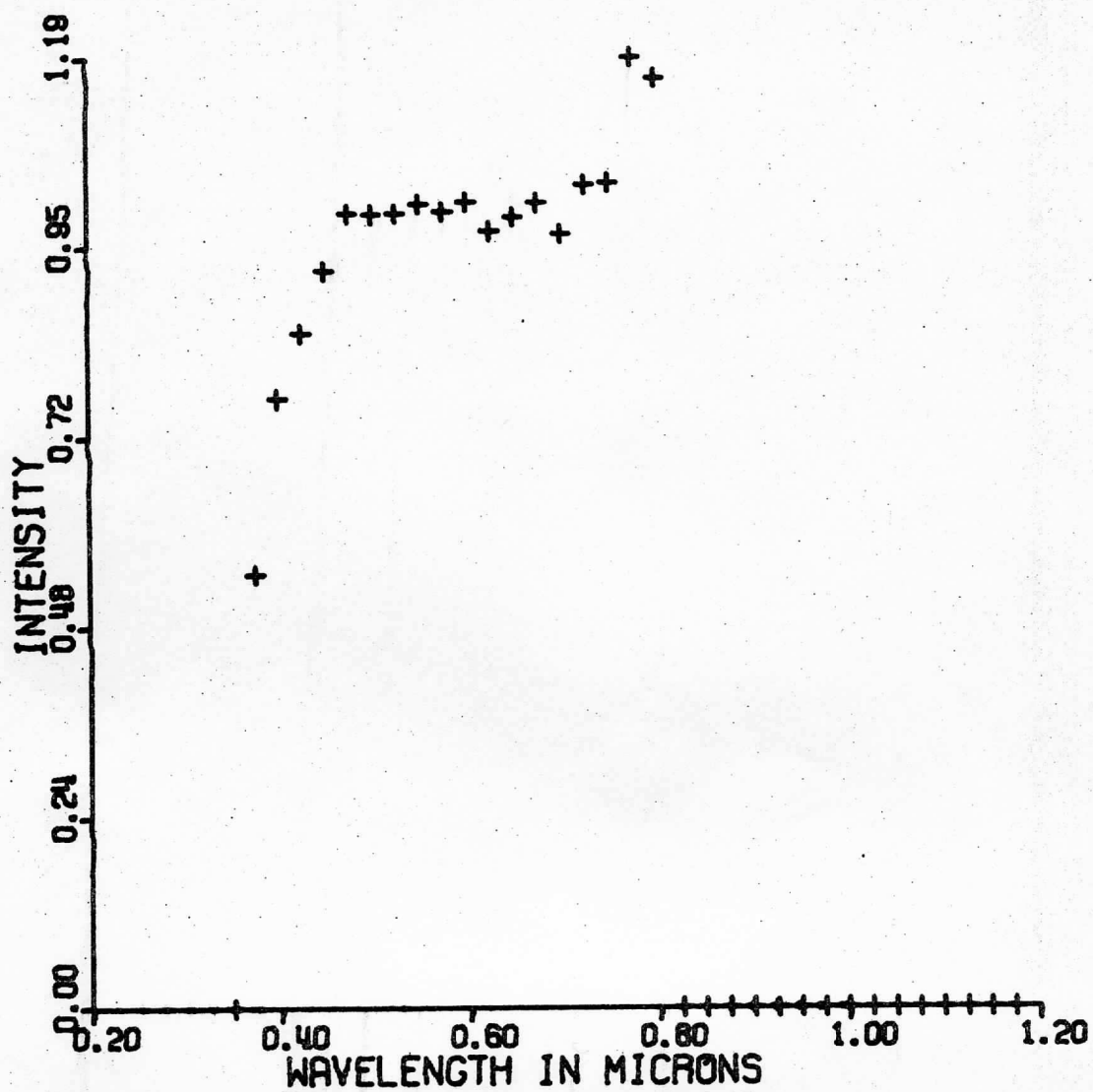
Figure 16. α Lyra spectrum from vidicon spectrometer with vidicon response (Figure 2) divided out.

removed. Note that the peak is shifted to a slightly longer wavelength and that the shape is generally broader to about 0.7 microns. To test the repeatability of the data, pairs of spectra of the same star were ratioed to each other. Results of one such pair are shown in Figure 17 (all ratios plotted are normalized to 1.0 at 0.575 microns). Figure 17a is the ratio of two Alpha Lyra spectra with similar airmasses (1.40/1.38), but different exposure times (5sec/1sec). If the response of the system were perfectly linear, that is, if intensity recorded from a given source is a linear function of the integration (exposure) time, the curve would be flat. It is obvious that it is not; however, the relatively flat region corresponds with the peak intensities of the spectra, so it may be that low level signals are nonlinear representations of the intensity received from the star. To test this idea, a 'pedestal' was set up under the spectrum. All intensities below a certain value would be ignored, and possibly, the nonlinear features of the curve would go away. Figures 17b and 17c show the results of installing pedestals of 300 and 400, respectively (the maximum intensity registerable is 4095). a pedestal of 300 seems to help from 0.5 to 0.8 microns, but a larger pedestal doesn't help at all. Figure 18 shows a similar ratio for two Xi 2 Ceti spectra with slightly different airmasses (1.67/1.32) and different exposure times (20sec/15sec). Once again the curve is relatively flat over the peak in incoming energy, this time from almost 0.4 to 0.8 microns. (Figure 19 is a



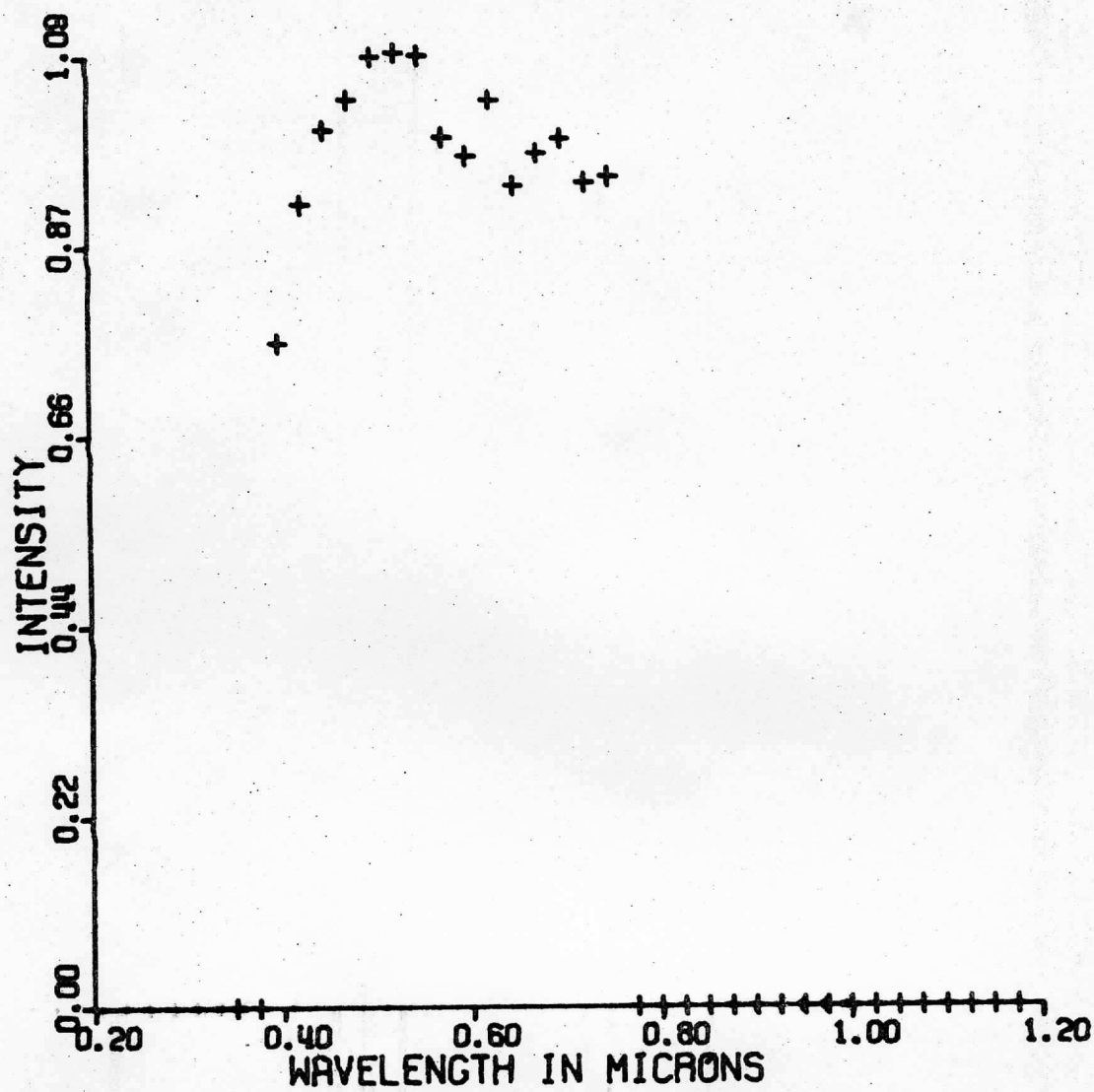
SALYR86 / SALYR83

Figure 17a. Ratio of two α -Lyra spectra, all elements above background included.



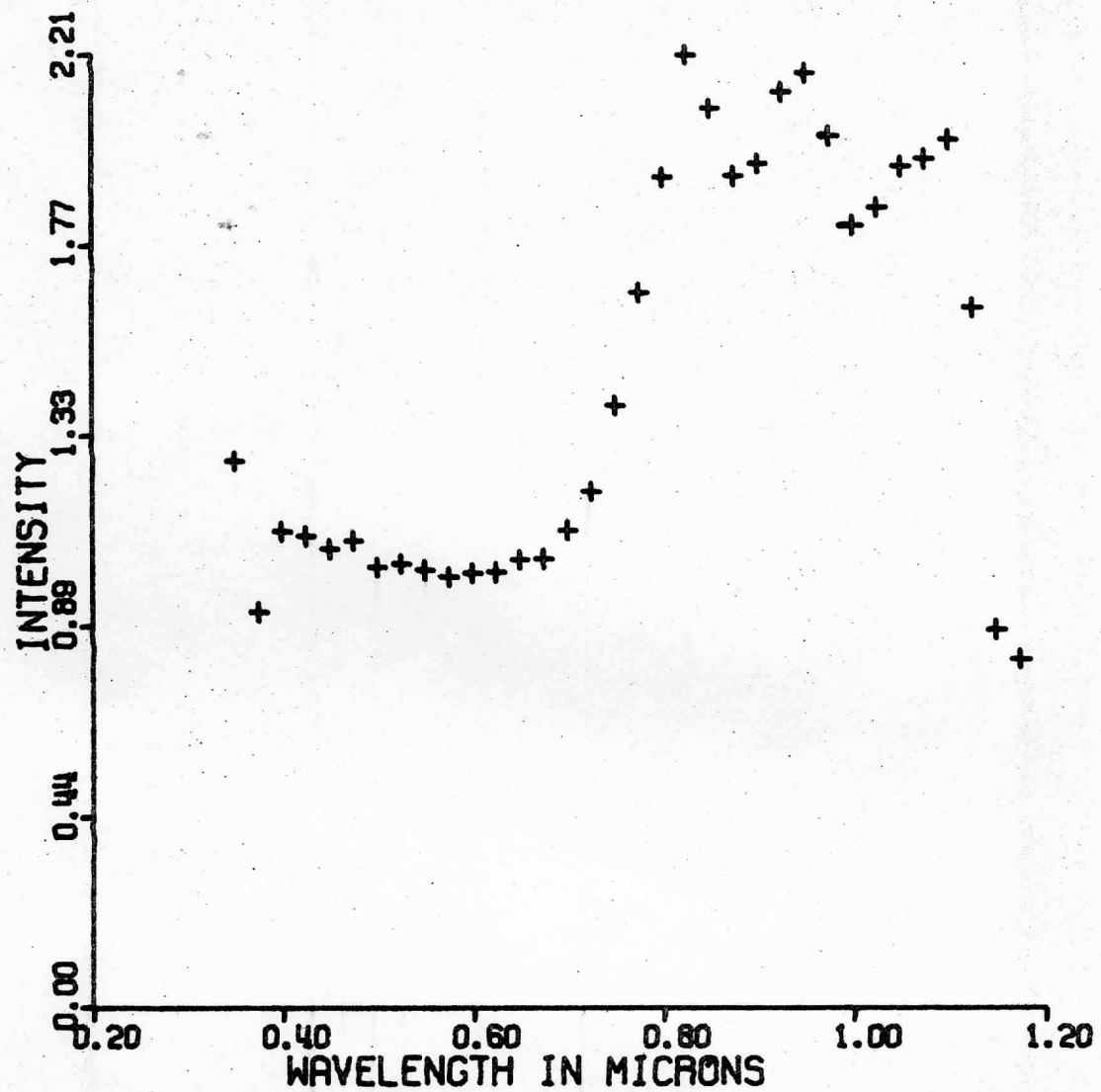
SALYR86 / SALYR83

Figure 17b. Ratio of same two α Lyra spectra,
this time including no elements less than 300.



SALYR86 / SALYR83

Figure 17c. Ratio of same two α Lyra spectra,
this time including no elements less than 490.

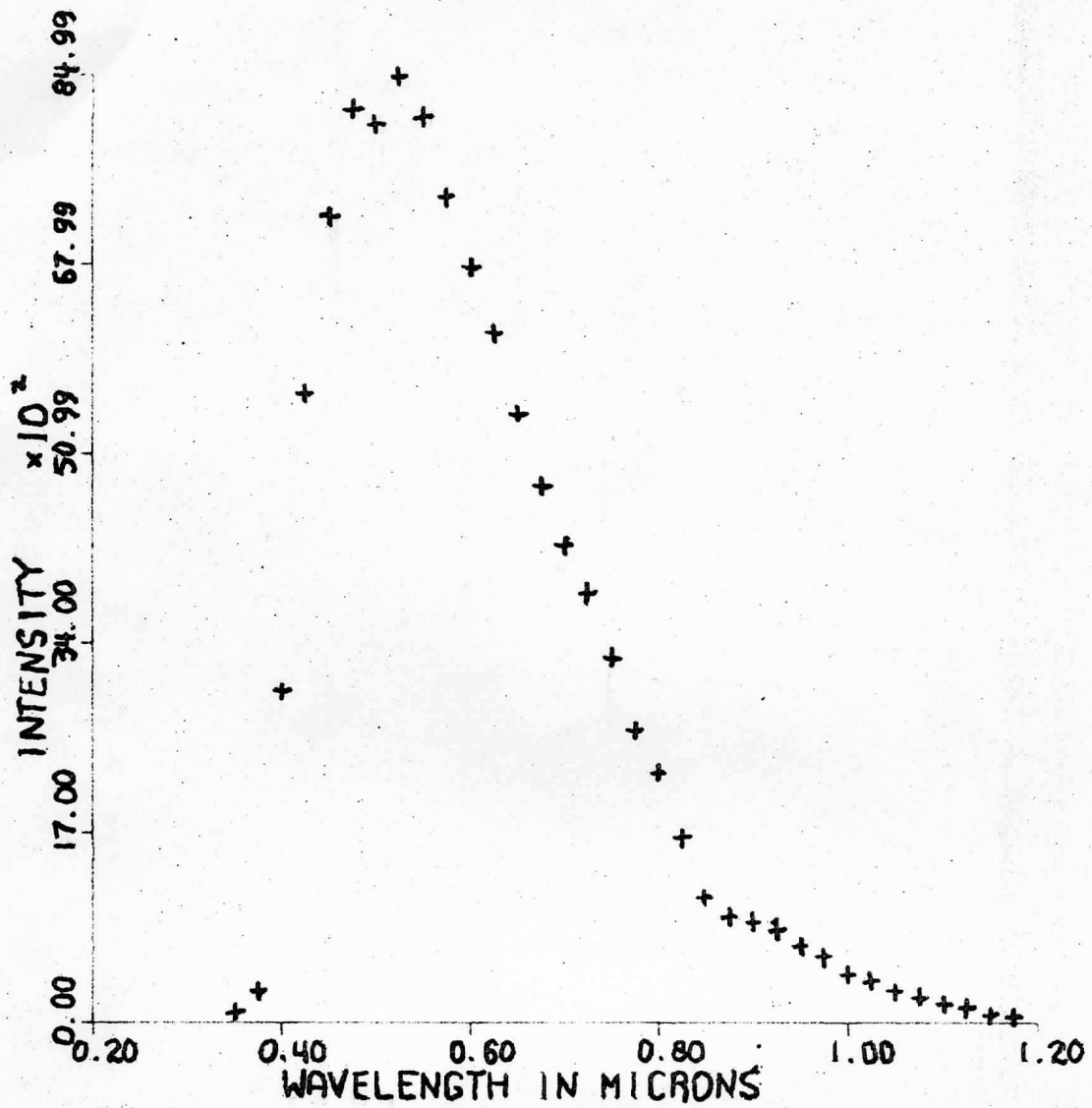


SXCT112 / SXCT124

Figure 18. Ratio of two ξ^2 Ceti spectra, including all image elements above background.

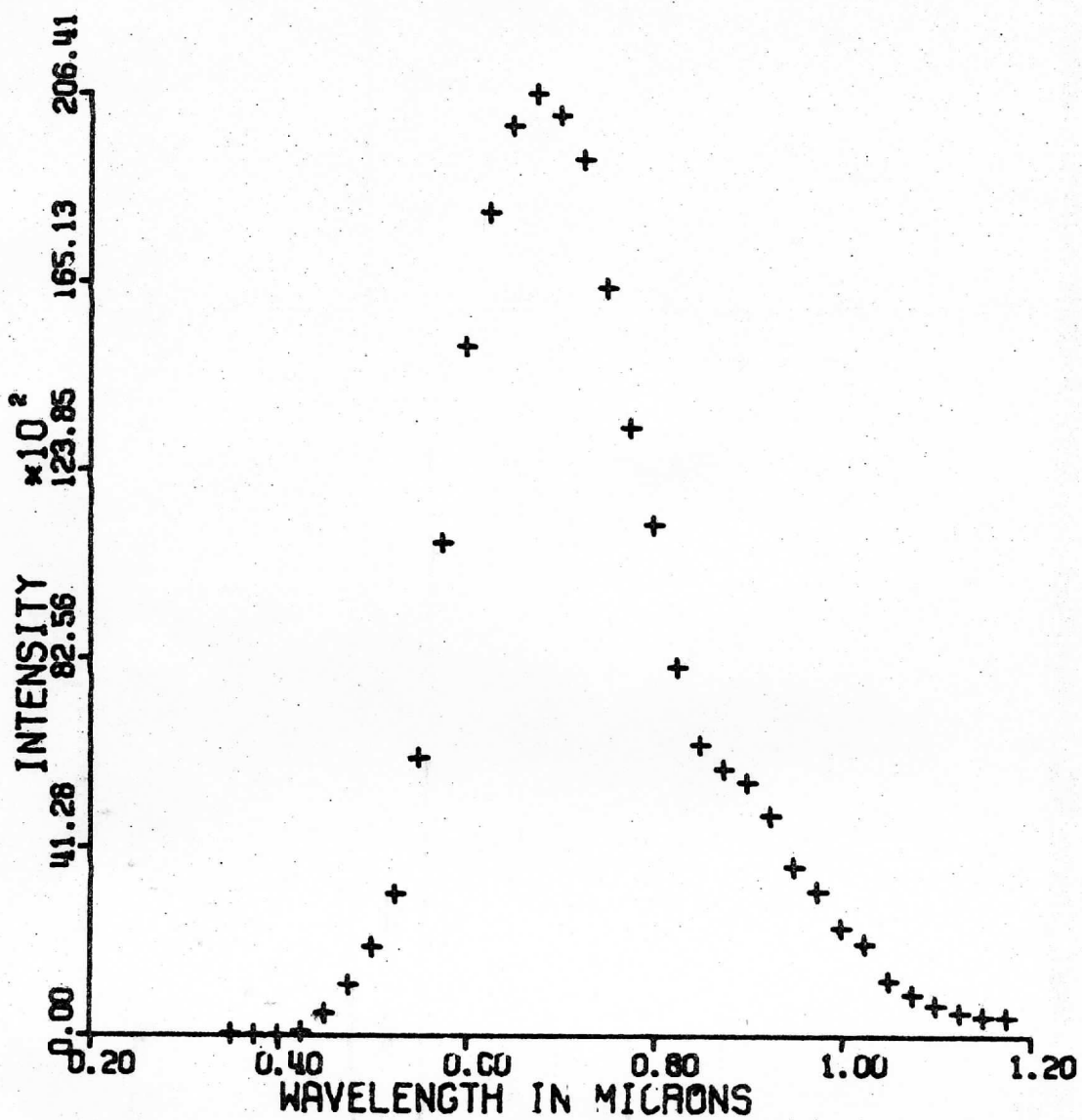
typical Xi 2 Ceti spectrum). this time, however, there is a smooth upturn which has some undetermined significance. Thus, star ratios seem to be usable, at best, from 0.4 to 0.8 microns.

Now that there is some idea as to the reliability range of the spectrometer, indefinite though it may be, the Mars spectra can be observed. Figure 20 is a typical Mars spectrum, summed over five vidicon elements down the slit. Note that the peak is in the red, rather than the blue like the two stars' spectra. This is because the stars are both of spectral type A0, while the sun, which is providing the light which is reflected from Mars is a cooler, redder type G. Figure 21 shows a saturated spectrum of Mars. The peak intensity of 4095 is surpassed from 0.5 to 1.0 microns, although around 1.1 microns, the signal is unsaturated. Originally it was thought that the unsaturated portions of a saturated spectrum could be used to extend the range of an unsaturated spectrum which had a very low signal beyond 1.1 microns. The data show, unluckily, that there is little or no overlap between the good signal from one and the good signal from the other type of spectrum. Once again, an attempt was made to do away with low, nonlinear signals with a pedestal. Figures 22a,b, and c show the progressive changes as pedestals of 300 and 400 are subtracted from the original spectrum. Ratios of Mars images seem to be more consistent than those of star images. Figures 23a,b, and c and 24a,b, and c are the results of ratioing different images of Mars to each other. The three images used



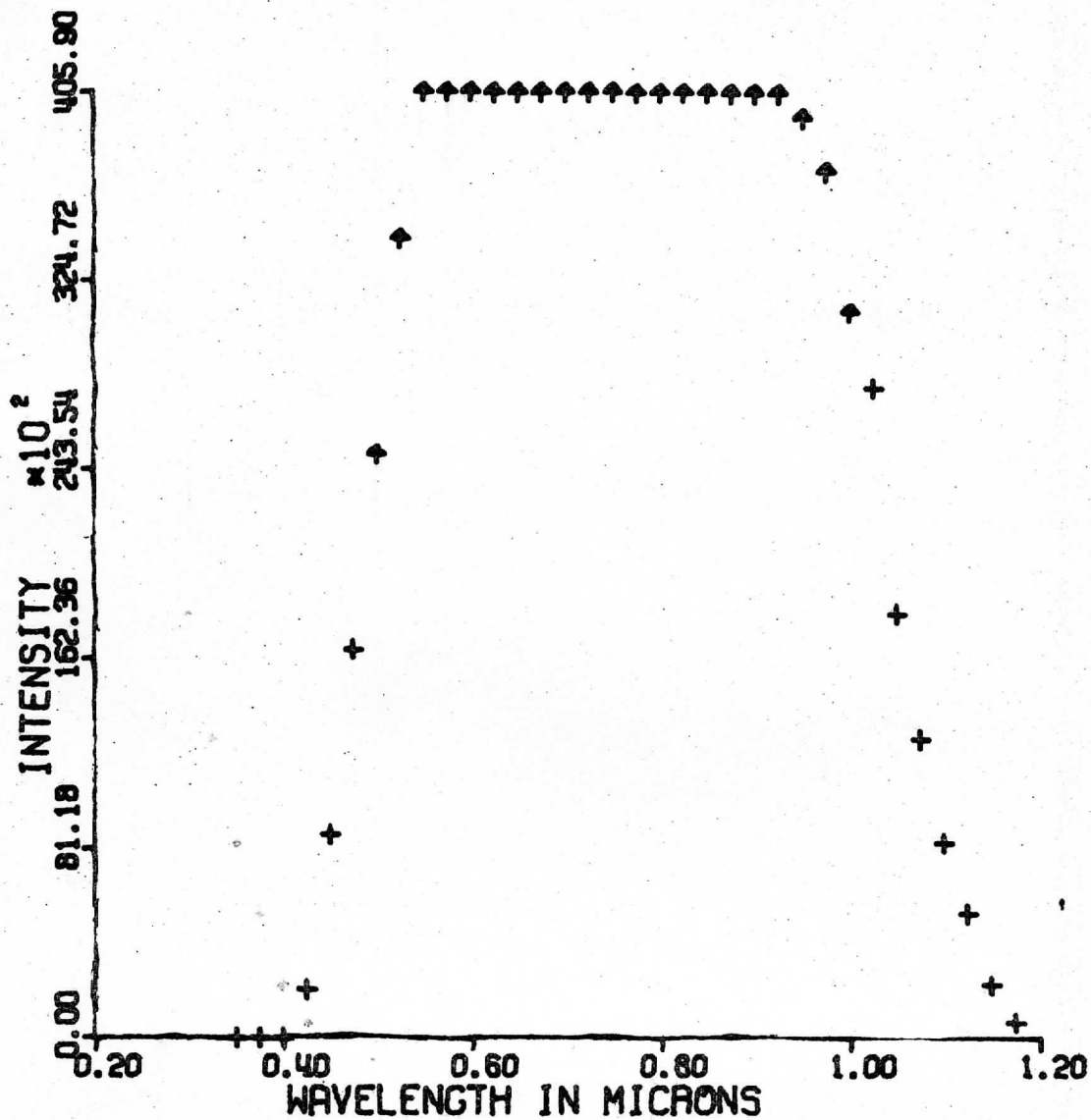
SXCT112 INTEG.

Figure 19. A typical ξ^2 Ceti spectrum. Note that the peak is at a longer wavelength and the shape is broader than α Lyra.



SMARSC-4 INTEG.

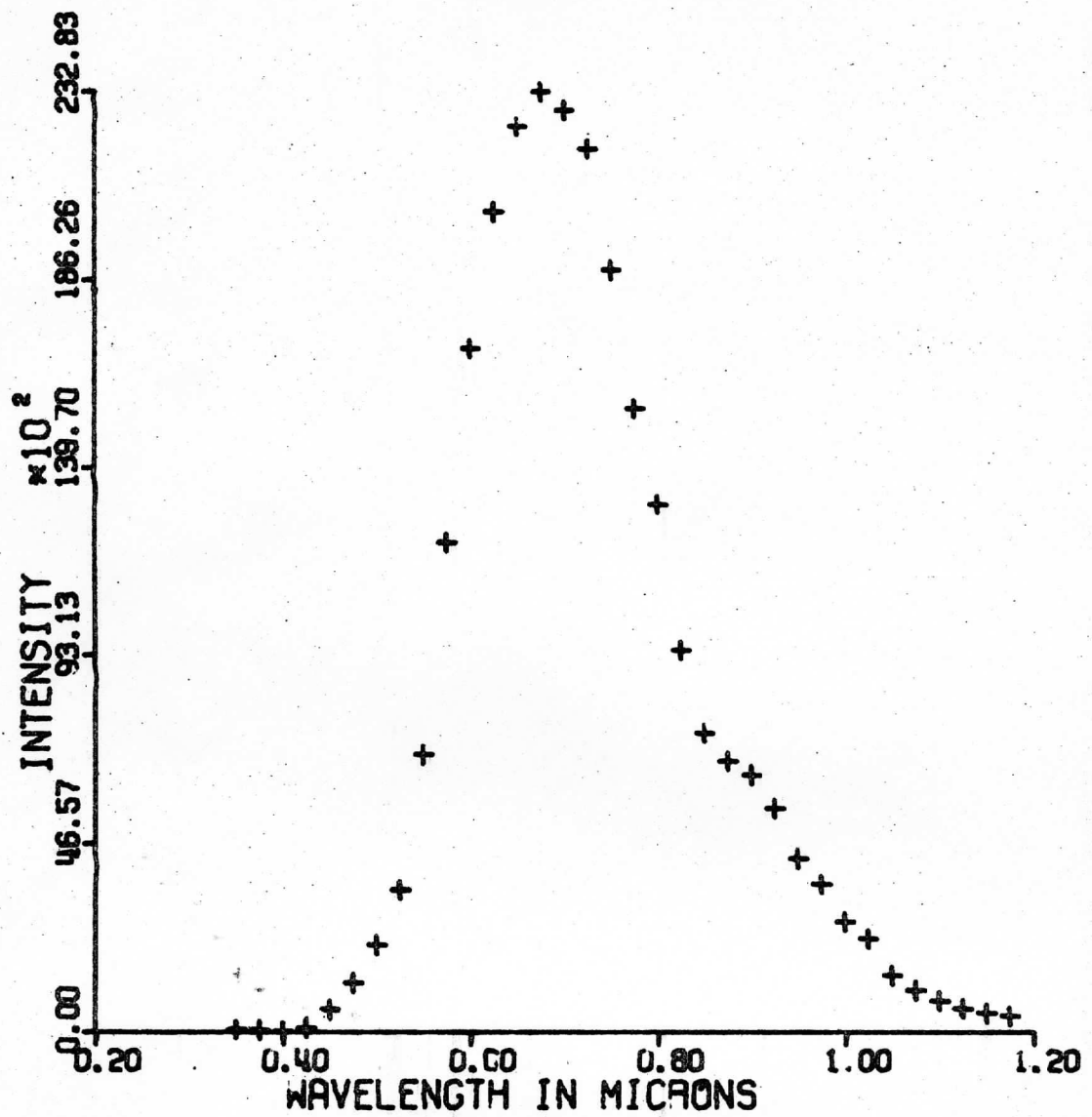
Figure 20. A typical Mars spectrum



SMARSC-5 INTEG.

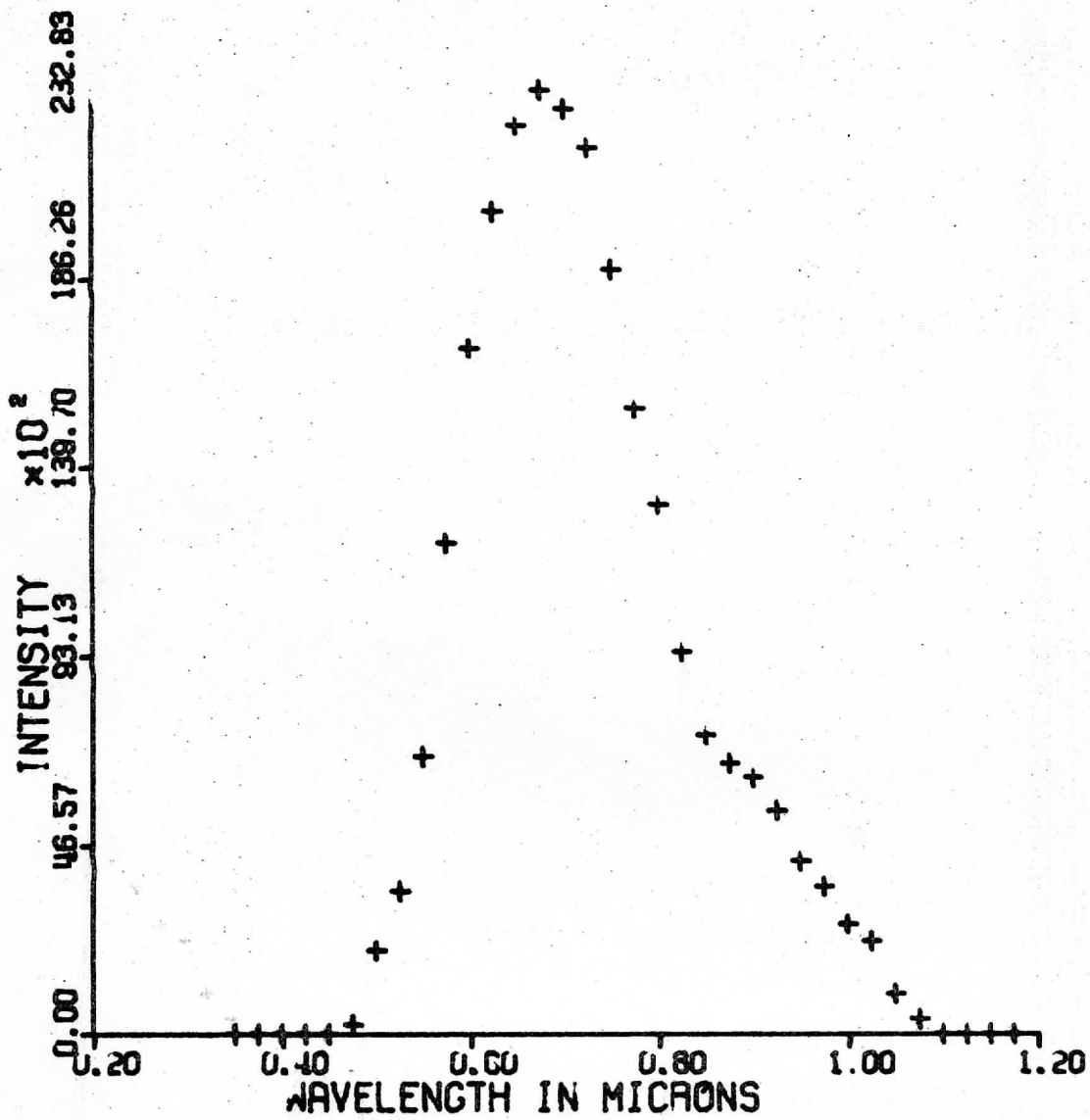
Figure 21. An overexposed spectrum of Mars.

Arrows indicate intensities reading greater than 4095 in at least one element of the image which went into the resolution element.



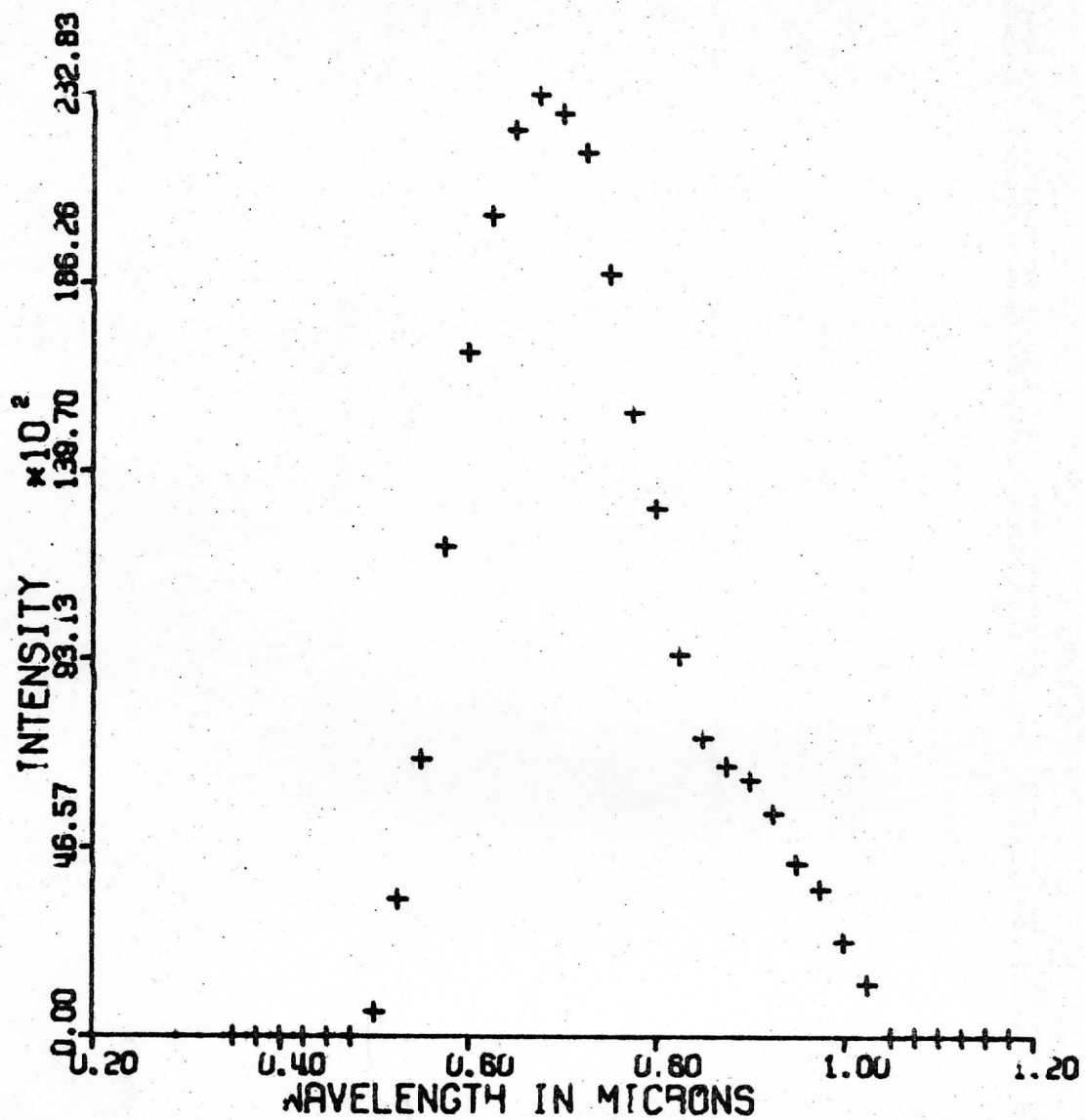
SMARSC-1 INTEG.

Figure 22a. Mars spectrum



SMARSC-1 INTEG.

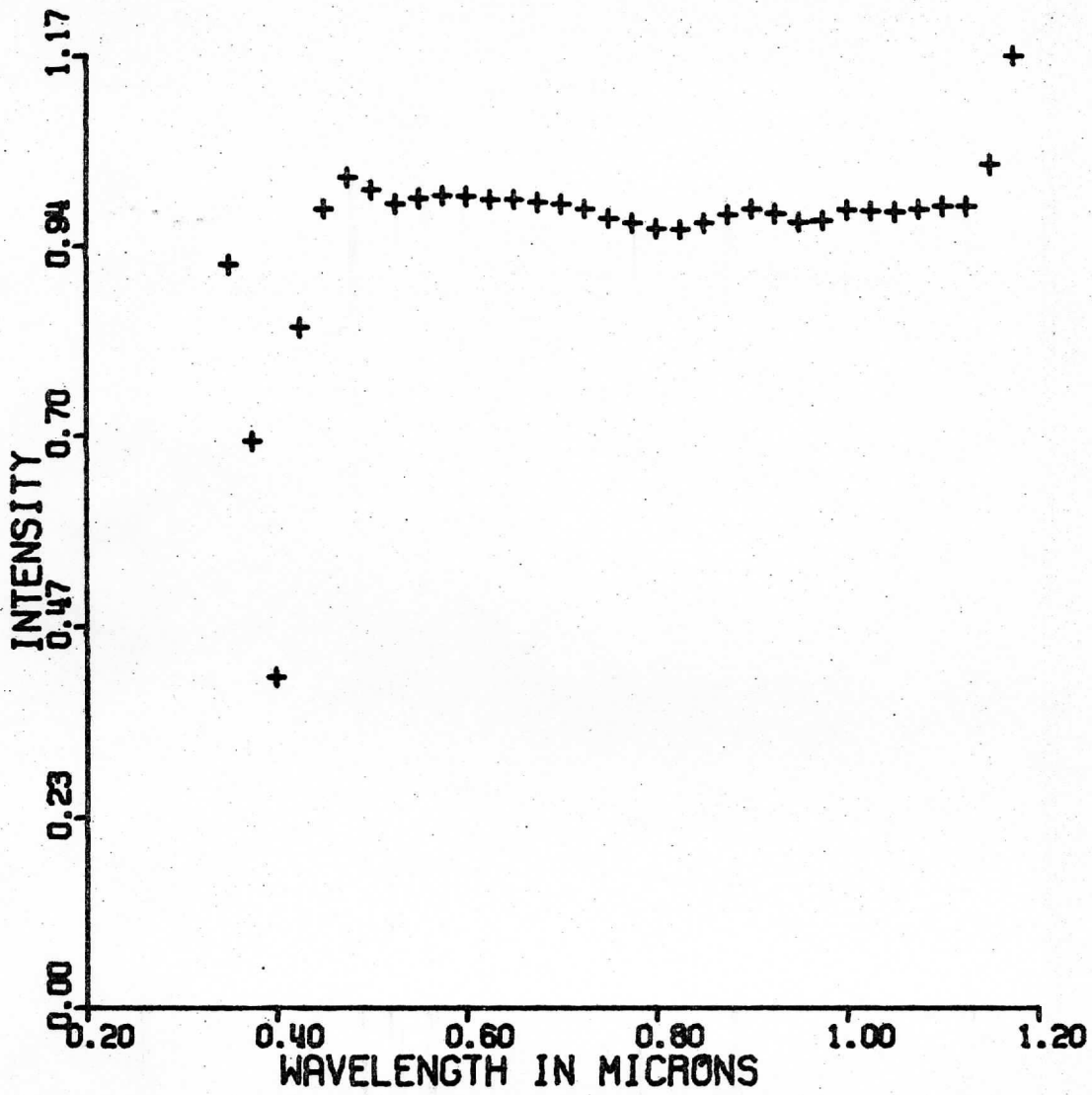
Figure 22b. Mars spectrum with pedestal of 300.



SMARSC-1 INTEG.

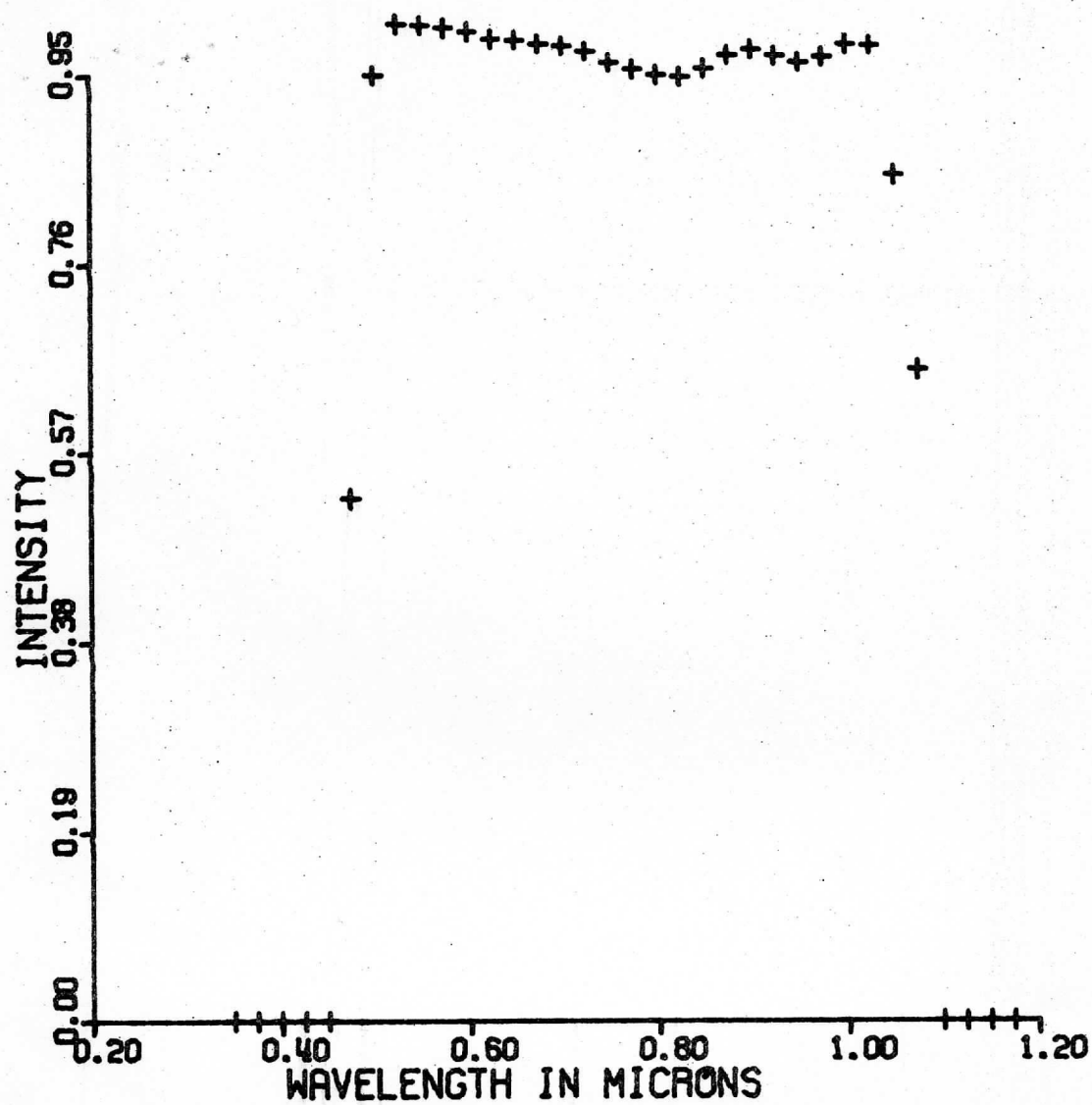
Figure 22c. The same Mars spectrum with a pedestal
of 400.

were taken within 15 minutes of each other. The same portion of the image was used in each case. Each is a one minute exposure. Note the flat curve from 0.5 to 1.1 micron, indicating better repeatability than for the stars, possibly due to more signal above a nonlinear level. As the pedestal is increased, some of the apparently good data is lost, but the noise is gone by the time a pedestal of 400 is used (c). The Mars spectra are probably recoverable.



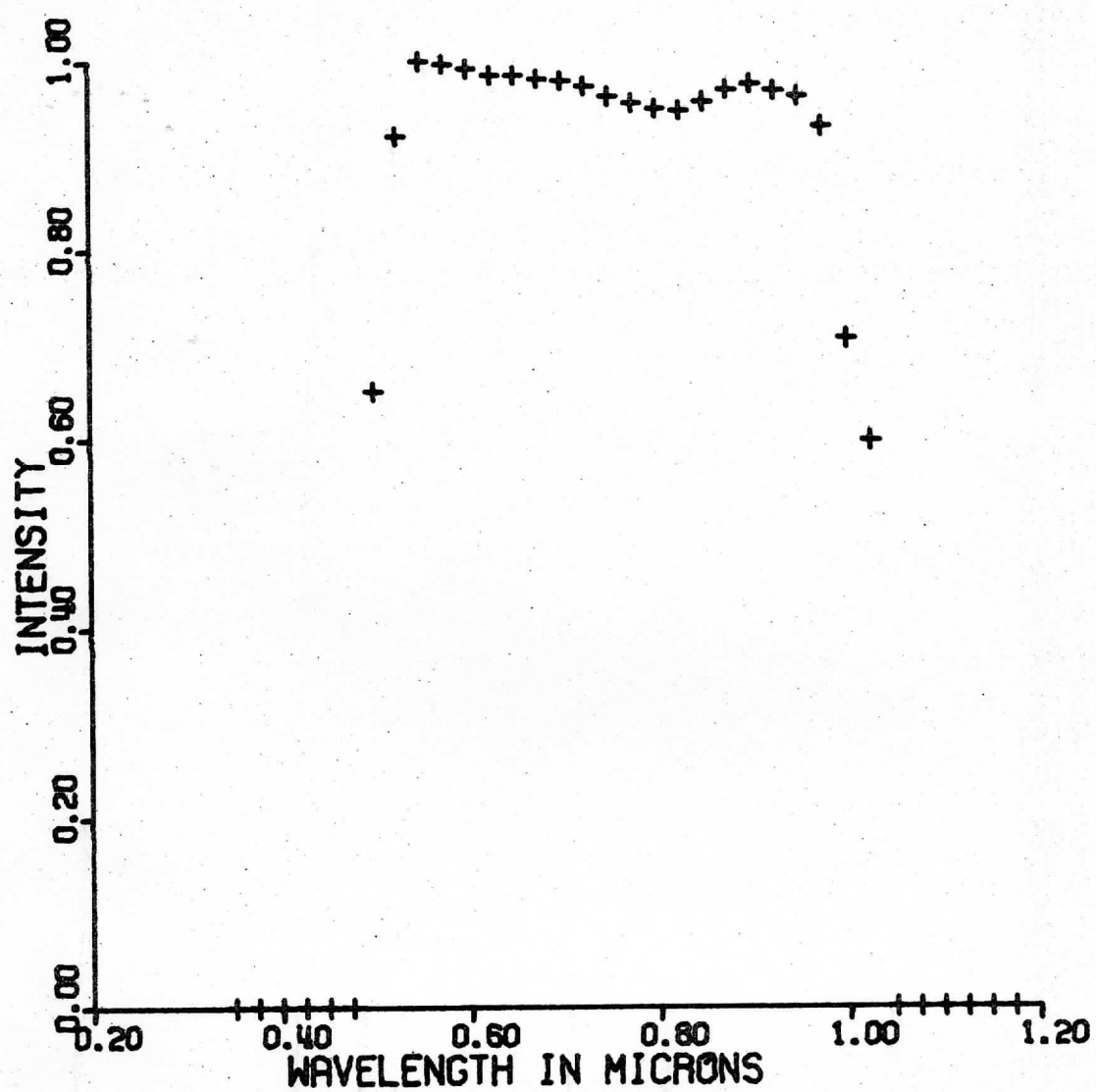
SMARSC-4 / SMARSC-1

Figure 23a. Ratio of two Mars spectra.



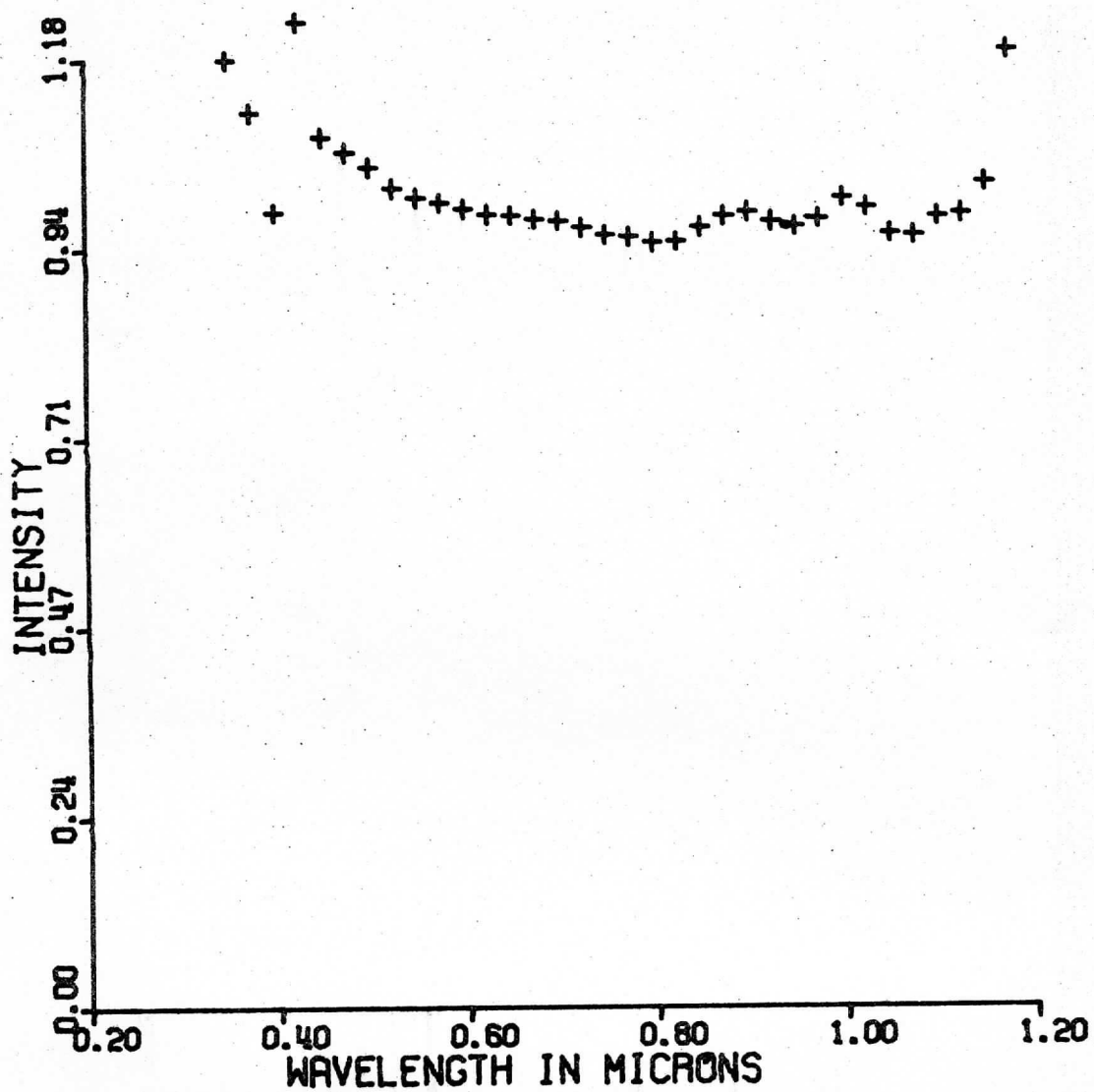
SMARSC-4 / SMARSC-1

Figure 23b. Ratio of two Mars spectra, each of which has a pedestal of 300.



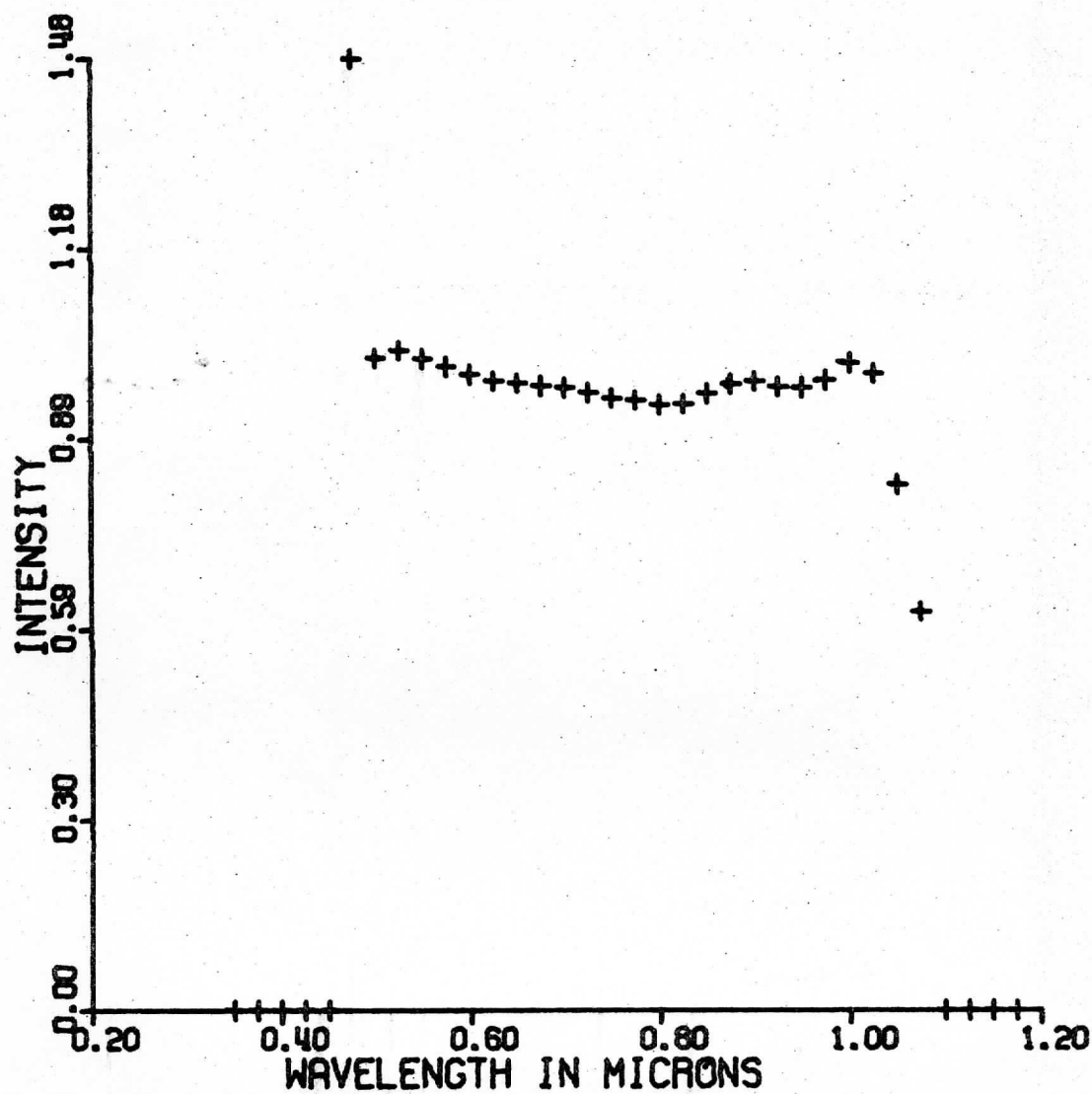
SMARSC-4 / SMARSC-1

Figure 23c. Ratio of same two Mars spectra, this time with a pedestal of 400 under each.



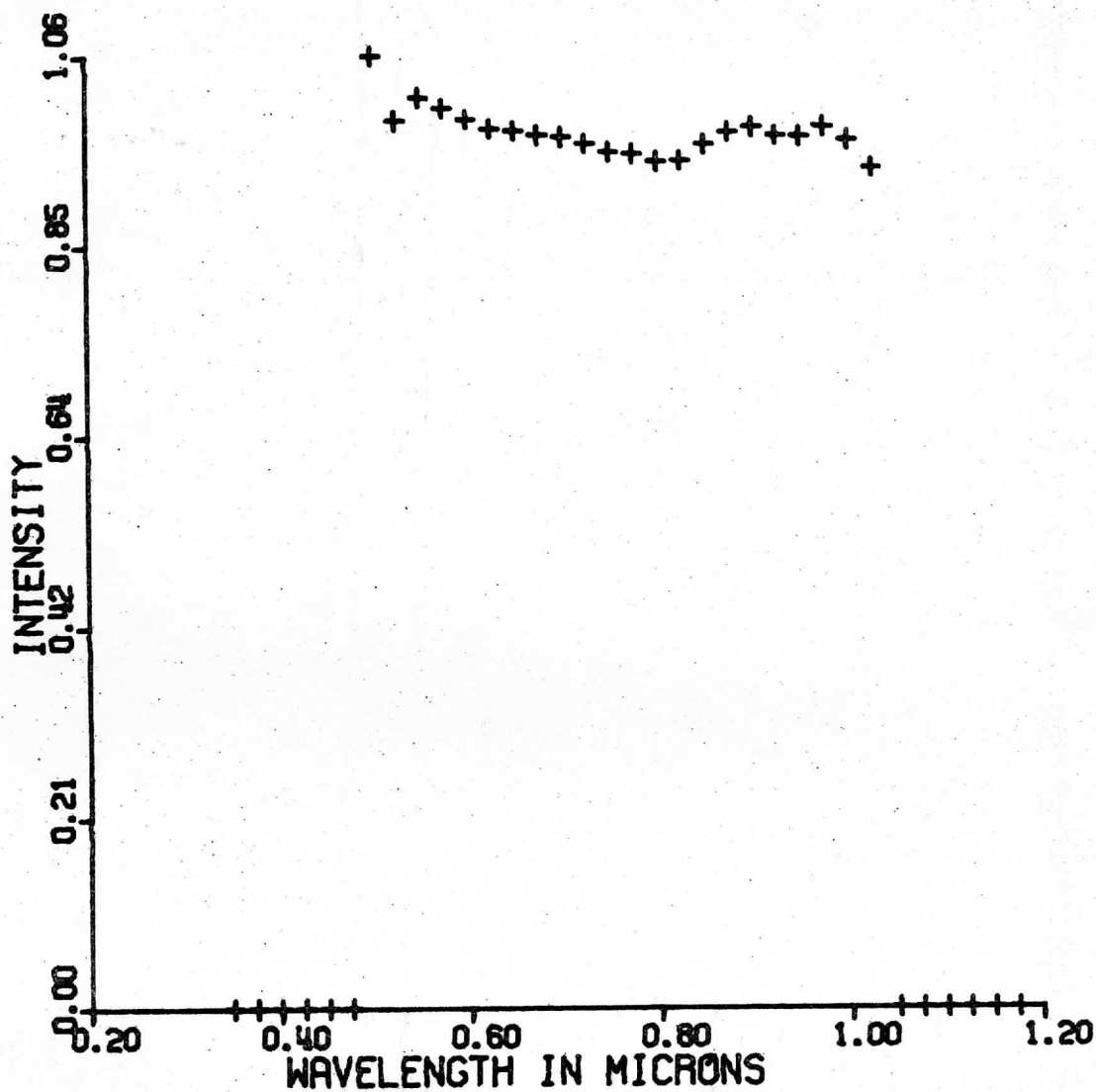
SMARSC-9 / SMARSC-1

Figure 24a. Ratio of two Mars spectra, without pedestals.



SMARSC-9 / SMARSC-1

Figure 24b. Ratio of two Mars spectra, each of which has a pedestal of 300.



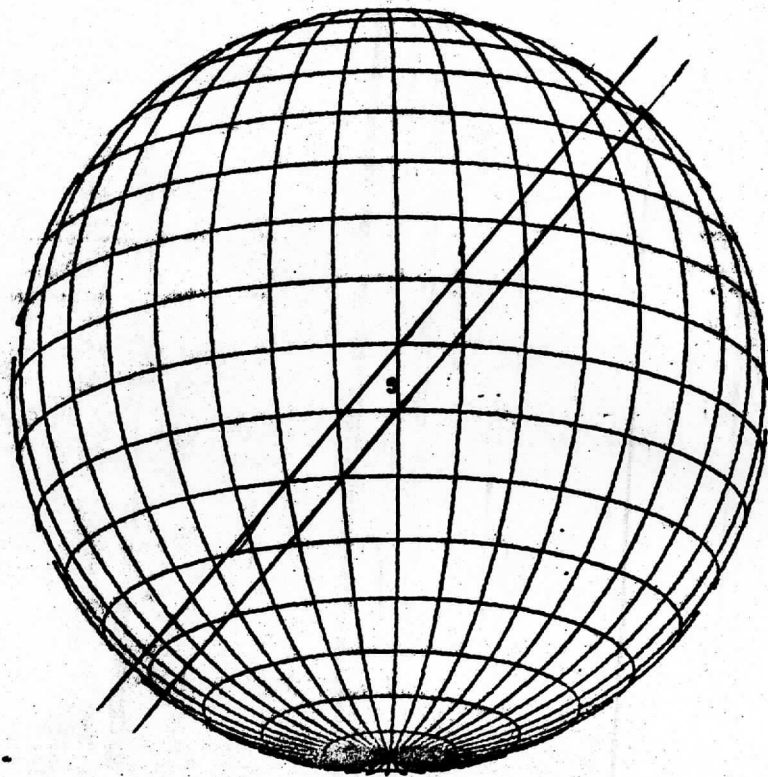
SMARSC-9 / SMARSC-1

Figure 24c. Ratio of same two Mars spectra, each of which now has a pedestal of 400.

V. Recommendations for Future Use of the Vidicon Spectrometer

Although it appears that it will be impossible to do spectral reflectivity work using the vidicon spectrometer due to an inability to meaningfully ratio stars and planets over a useful range, the instrument has advantages which will make it worthwhile to develop it. The combination of good spectral resolution (250 angstroms or better, compared to 300 angstroms for a filter photometer), with complete spectral coverage and high spatial resolution indicate much promise. It appears that the limiting factor will be the response function of the vidicon tube, with its nonlinearities in wavelength and intensity. Once more lab work is done to quantify knowledge about this problem, the instrument will be ready to gather more data. Another problem which may affect the star spectra is the problem of differential diffraction of the star's light by the earth's atmosphere. Different wavelengths, diffracted at slightly different angles would show up at different positions in the smeared out star spectrum, and if the slit is smaller than the apparent diameter of the star, part of the star's spectrum would be lost, in a wavelength-preferential manner. The solution is to widen the slit; although the spectral resolution at the vidicon would be reduced, the spectrum would be much more reliable. But what about the Mars data from Mauna Kea? With the high spatial resolution and apparent good response of the vidicon, something should be recoverable. The planet in the slit occupies

up to 35 elements in a vidicon column when it is about 23 arc seconds in diameter, and the slit is two elements wide, so, with good seeing of 1.5 seconds or less, there are fifteen spectra per spectrometer image. Luckily, the slit passes over some photometer spots that were taken within days of the vidicon spectrometer run, allowing relative reflectivities to be obtained, basically extending the photometer data for more complete surface coverage. For example, Figure 25 shows the position of the slit on the planet's disk during one run. This one slit passes through the Coprates canyon as well as a large dust storm to the southwest of Coprates. Using a photometer spot as a standard and modifying resolution to match the photometer, some interesting data should be forthcoming.



MARS
VIDSPEC B
1 OF 4
OCT. 17, 1973
T = 11:14 UT
LAT. = -17.2
LONG. = 51.8
DIA. = 21.47 SEC

Figure 25. Position of one set of spectra across the disk of Mars. Latitude and longitude of the sub-earth point, S, given.

REFERENCES

- Adams, J. B. (1968) "Lunar and Martian Surfaces: Petrologic Significance of Absorption Bands in the Near-Infrared," Science 159, p. 1453-1455.
- Adams, J. B. and T. B. McCord (1969) "Mars: Interpretation of Spectral Reflectivity of Light and Dark Regions," JGR 74, p. 4851-4856.
- Crowell, M. H. and E. F. Labuda (1969) "The Silicon Diode Array Camera Tube," Bell System Technical Journal, May-June 1969, p. 1481-1528.
- Dollfus, A. (1961) "Polarization Studies of Planets," Chapter 9 in Planets and Satellites, edited by G. P. Kuiper and B. M. Middlehurst, (Chicago: University of Chicago Press).
- Hovis, W. A., Jr. (1965) "Infrared Reflectivity of Iron Oxide Minerals," Icarus 4, p. 425-430.
- Kunin, J. S. (1972) "A Technique for Two-Dimensional Photoelectronic Astronomical Imaging, With Application to Lunar Spectral Reflectivity Studies," M.S. Thesis, M.I.T., September 1972.
- McCord, T. B., and J. Bosel. (1973) "Silicon Vidicon Astronomy at MIT," presented at the symposium, "Astronomical Observations with Television-Type Sensors," held May 15-17, 1973, at the University of British Columbia.
- McCord, T. B., J. H. Elias, and J. A. Westphal (1971) "Mars: The Spectral Albedo (0.3-2.5 μ) of Small Bright and Dark Regions," Icarus 14, p. 245-251.
- McCord, T. B. and J. A. Westphal (1971) "Mars: Narrow-Band Photometry, from 0.3 to 2.5 Microns, of Surface Regions During the 1969 Apparition," Astrophys.J. 168, p. 141-153.
- McCord, T. B. and J. A. Westphal (1972) "Two-Dimensional Silicon Vidicon Astronomical Photometer," Applied Optics 11, p. 522-526.
- Sagan, C., J. P. Phaneuf, and M. Ihnat (1965) "Total Reflection Spectro-photometry and Thermogravimetric Analysis of Simulated Martian Surface Materials," Icarus 4, p. 43-61.
- Tull, R. G. (1966) "The Reflectivity Spectrum of Mars in the Near-Infrared," Icarus 5, p. 505-514.

Determination of Martian Surface Spectral Reflectivity from 0.4 to 1.1μ
Using a Vidicon Spectrometer

A Proposal for a thesis toward the degree of Master of Science

By Douglas J. Mink

I propose to analyze the spectral reflectivity of Mars from 0.4 to 1.1μ using the vidicon spectrometer system developed at the MIT Planetary Astronomy Laboratory. This system consists basically of a slit at the focus of a telescope, from which light goes through a low resolution prism. The spectrum produced is imaged on a vidicon image tube which is read out onto magnetic tape. The image produced has wavelength nonlinearily along one axis and spatial variation along the slit as the other axis. A prism dispersion function is used to calibrate wavelength to image column coordinate, and a photograph of the slit superimposed on the telescope image of the planet is used to determine spatial position.

About one hundred spectra were taken at Mauna Kea Observatory during the opposition of Mars in October of 1973 by members of the Planetary Astronomy Laboratory staff. Reduction of the data involves ratioing the intensity of light received from the planet, through known standard stars, to the sun's emitted radiation, thus obtaining the reflectivity of the planet's surface as a function of wavelength. This function has been shown to be an indication of the composition of the surface. Analysis has included hand-reduction of spectra and development of a computer program to plot a coordinate grid for a planetary disk from physical ephemeris data. A computer reduction system is being developed to handle the data.

Geological implications of the reflectivity spectra will be discussed, based on comparison with spectral reflectivity analysis of various minerals. Mineral content of Martian surface materials will be discussed in relation to various theories of Mars' composition, although extensive interpretation is beyond the scope of this thesis.